Cell Reports
Medicine

Article

Genetic and pharmaceutical targeting of HIF1α allows combo-immunotherapy to boost graft vs. leukemia without exacerbation graft vs. host disease

Graphical abstract

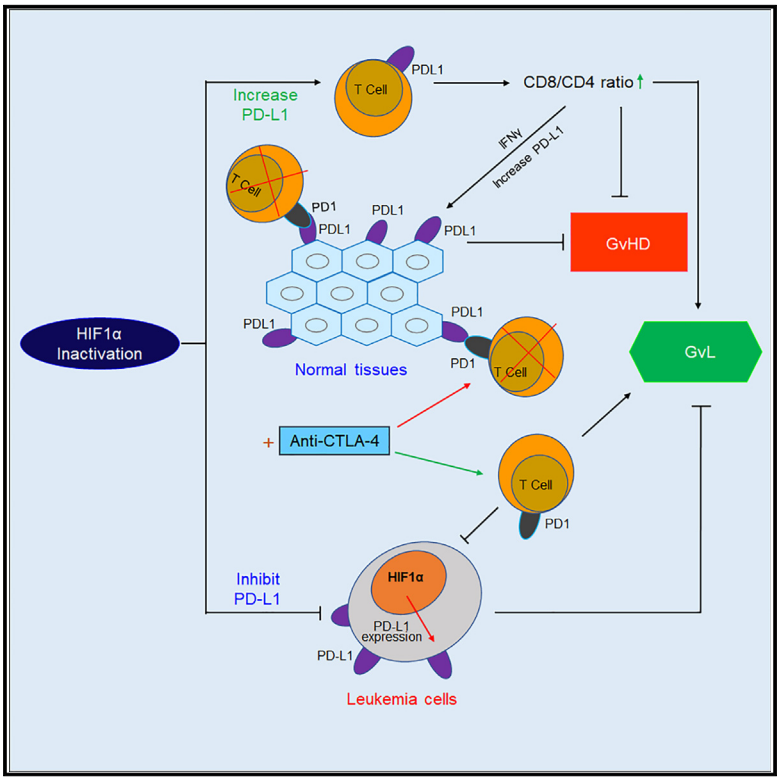

Authors

Christopher Bailey, Yuanyi Wei, Jinsong Yan, ..., Yan Liu, Yang Liu, Yin Wang

Correspondence

yanliu@ihv.umaryland.edu (Y.L.), yangl@oncoc4.com (Y.L.), yin.wang@ihv.umaryland.edu (Y.W.)

In brief

Anti-PD1/-PDL1 causes severe GVHD in patients who have had a bone marrow transplant (BMT). Bailey et al. show that HIF1α inhibition suppresses leukemia cell PDL1 while enhancing donor T cell-mediated PDL1 on host tissues, which uncouples GVHD and GVL and safely potentiates anti-CTLA4. Thus, HIF1α targeting may enable effective cancer immunotherapy for BMT recipients.

Highlights

- HIF1α in donor T cells drives GVHD in allo-BMT but is dispensable for GVL
- Inhibiting HIF1α in T cells increases IFNγ-mediated host tissue PDL1 expression
- Inhibiting HIF1α in leukemia cells suppresses PDL1 and potentiates GVL
- HIF1α inhibitor+ipilimumab combo allows PDL1/CTLA4 co-targeting without lethal GVHD

Bailey et al., 2023, Cell Reports Medicine *4*, 101236
November 21, 2023
https://doi.org/10.1016/j.xcrm.2023.101236

CellPress

Cell Reports Medicine

CellPress
OPEN ACCESS

Article

Genetic and pharmaceutical targeting of HIF1α allows combo-immunotherapy to boost graft vs. leukemia without exacerbation graft vs. host disease

Christopher Bailey,[1] Yuanyi Wei,[1] Jinsong Yan,[2] Dan Huang,[2] Peng Zhang,[3] Chong Qi,[4] Christopher Lazarski,[5] JuanJuan Su,[1] Fei Tang,[1] Chun-shu Wong,[5] Pan Zheng,[1,6] Yan Liu,[1,*] Yang Liu,[1,6,*] and Yin Wang[1,7,*]

[1]Division of Immunotherapy, Institute of Human Virology, Department of Surgery and Comprehensive Cancer Center, University of Maryland School of Medicine, Baltimore, MD 21201, USA

[2]Department of Hematology, The Second Hospital of Dalian Medical University, Dalian, China

[3]Department of Neurosurgery, Beijing Children's Hospital, Capital Medical University, National Cancer for Children's Health, Beijing, China

[4]Institute of Translational Medicine, The First Hospital, Jilin University, Changchun, Jilin 130061, China

[5]Center for Cancer and Immunology Research, Children's Research Institute, Washington, DC 20010, USA

[6]OncoC4, Inc., Rockville, MD 20852, USA

[7]Lead contact

*Correspondence: yanliu@ihv.umaryland.edu (Y.L.), yangl@oncoc4.com (Y.L.), yin.wang@ihv.umaryland.edu (Y.W.)

https://doi.org/10.1016/j.xcrm.2023.101236

SUMMARY

Despite potential impact on the graft vs. leukemia (GVL) effect, immunotherapy targeting CTLA-4 and/or PD-1 has not been successfully combined with bone marrow transplant (BMT) because it exacerbates graft vs. host disease (GVHD). Here, using models of GVHD and leukemia, we demonstrate that targeting hypoxia-inducible factor 1α (HIF1α) via pharmacological or genetic approaches reduces GVHD by inducing PDL1 expression on host tissue while selectively inhibiting PDL1 in leukemia cells to enhance the GVL effect. More importantly, combination of HIF1α inhibition with anti-CTLA-4 antibodies allows simultaneous inhibition of both PDL1 and CTLA-4 checkpoints to achieve better outcomes in models of mouse and human BMT-leukemia settings. These findings provide an approach to enhance the curative effect of BMT for leukemia and broaden the impact of cancer immunotherapy.

INTRODUCTION

Allogeneic hematopoietic stem cell transplantation (allo-HSCT) is a curative option for hematopoietic malignancies.[1] However, the success of allo-HSCT is impeded by graft vs. host disease (GVHD) and leukemia relapse.[2–4] Donor bone marrow (BM)-derived lymphocytes are critical for preventing leukemia relapse—a phenomenon referred to as the graft vs. leukemia (GVL) effect. On the other hand, GVHD, which manifests as the destructive activities of donor lymphocytes on healthy host tissues, is a leading cause of morbidity and mortality associated with allo-HSCT.[5,6] The prospect of abrogating GVHD without jeopardizing GVL is considered a Holy Grail for allo-HSCT. However, efforts toward this have had limited success, as it is challenging to mechanistically uncouple destructive activities of donor lymphocytes toward cancerous vs. non-cancerous host tissues.[5–7]

The pioneering work in developing immunotherapy targeting programmed cell death-1 (PD1) and PDL1[8–10] led to the most important breakthrough in cancer therapy, with rapidly expanding indications of anti-PD1/-PDL1 antibodies adopted for treatment of hematological and non-hematological malignancies.[11] However, the current approach that overcomes tumor evasion of host immunity also disables the immune tolerance checkpoint, leading to significant immunotherapy-related adverse events (irAEs), particularly when used in conjunction with anti-CTLA-4 antibodies. In hematological malignancies, immune checkpoint inhibitors (ICIs) have been examined as experimental therapies in settings of post-allo-HSCT relapse[12–14] or as a bridge to allo-HSCT.[13,15,16] However, these strategies will be secondary to overactivate the immune system and exacerbate GVHD.[17,18] Patients with relapsed/refractory lymphoma have shown high response rates to anti-PD1 antibodies, but most eventually progress.[19,20] Anti-PD1 antibodies were proposed as a bridge to allo-HSCT, but in response to the resulting severe acute GVHD observed in the clinical study,[18,21,22] the FDA issued a warning against treating HSCT patients with anti-PD1.[23]

We have shown in syngeneic solid tumor models that targeting hypoxia-inducible factor 1α (HIF1α) in combination with anti-CTLA-4 antibodies abrogates PDL1-mediated immune evasion in the tumor microenvironment but confers protection from irAEs by increasing PDL1 levels in non-tumor host tissues.[24] Although loss of PDL1 exacerbated GVHD in mice,[25] whether PDL1 supplementation can suppress GVHD has not been investigated. Whether HIF1α drives PDL1 expression in normoxic leukemia cells that protects them from elimination by allogeneic T cells is also unknown. Here, we show that, following bone marrow transplant (BMT), HIF1α functions as a molecular switch to drive GVHD while suppressing GVL through differentially regulating

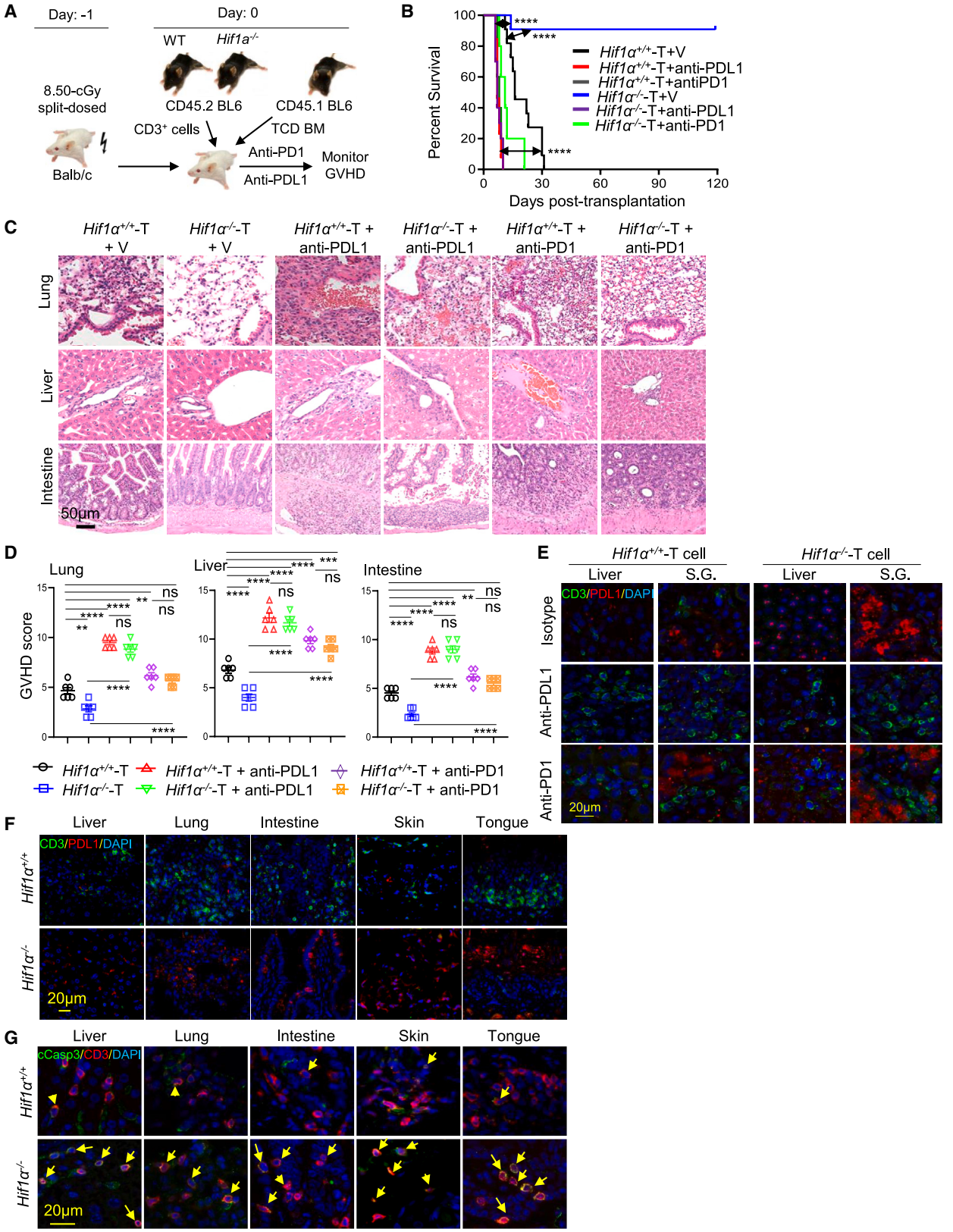

(legend on next page)

PDL1 on leukemia vs. non-tumor host tissues. Importantly, HIF1α inhibition is sufficient to protect against GVHD even with concurrent anti-CTLA-4 therapy with ipilimumab. HIF1α inhibitors plus anti-CTLA-4 antibodies allow targeting both PD(L)1 and CTLA-4 immune checkpoints in the BMT setting.

RESULTS

HIF1α target genes are highly expressed in the PBMCs and BM cells of patients with GVHD

We used gene set enrichment analysis (GSEA) on a published dataset[26] to identify gene sets enriched in T cells from patients with severe GVHD, finding 7 hallmark gene sets with HIF1α target genes most significantly enriched (Figures S1A–S1C). We collected BM or peripheral blood mononuclear cell (PBMC) samples from 19 allogeneic allo-HSCT recipients, comprising patients with GVHD or non-GVHD patients matched for age, gender, and time between transplantation and sample collection (Tables S1 and S2). We analyzed mRNA levels of fifteen HIF1α target genes based on their enrichment in GVHD patient samples,[27–29] using the primers listed in Table S3. Evaluable results were obtained from ten genes. Among them, expression of *GLUT1*, *MCL1*, *HK1*, *SNAIL*, *PKM*, *HOOK3*, and *TIMP*1 genes were significantly enhanced in patients with GVHD (Figure S1D).

Targeted mutation of *Hif1a* in T cells suppresses GVHD

We generated $Hif1a^{-/-}$ T cells by crossing $CD4^{cre}$ mice with $Hif1a^{flox/flox}$ mice. We then performed allogeneic BMT into BALB/c mice using CD45.1 C57BL/6 T cell-depleted (TCD) BM mixed with wild-type (WT) or $Hif1a^{-/-}$ T cells from CD45.2 C57BL/6 mice (Figure S2A). We analyzed HIF1α levels among fluorescence-activated cell sorting (FACS)-sorted donor T cells (Figure S3A) by western blot. While WT donor T cells (Figure S3B) expressed no detectable levels of HIF1α prior to transplantation, HIF1α was accumulated in donor T cells from the spleen 14 days post-BMT (Figure S2B), indicating that HIF1α is accumulated in donor T cells in GVHD.

We recorded body weights, clinical scores, and survival of mice receiving WT or $Hif1a^{-/-}$ T cells. WT T cells caused rapid mortality, while 80% of the $Hif1a^{-/-}$ T cell recipients survived the observation period (Figure S2C). WT T cell recipients showed reduced body weights (Figure S2D) and increased GVHD scores based on fur texture, skin integrity, activity, body weight, and posture (Figure S2E). Histology showed less inflammation, tissue injury, and donor T cell infiltration for $Hif1a^{-/-}$ T cell recipients in organs such as liver, lung, skin, intestine, and tongue (Figures S2F–S2H), indicating that *Hif1a* in donor T cells is essential for GVHD.

We have shown the small molecule echinomycin to be a potent HIF1α inhibitor in several models.[24,30–35] Echinomycin significantly reduced GVHD scores and prolonged survival for WT, but not $Hif1a^{-/-}$, T cell recipients (Figures S2I and S2J), implying that targeting *Hif1a* in T cells alone is sufficient to confer GVHD protection.

Blockade of PD1/L1 pathway abrogated GVHD suppression induced by HIF1α targeting

Antibodies that block PD1/PDL1 worsen GVHD in both mice and humans.[17,25,36] We tested the effects of anti-PD1 or anti-PDL1 antibodies in WT or $Hif1a^{-/-}$ T cell recipients (Figure 1A). Consistent with an earlier study,[25] anti-PD1 or anti-PDL1 exacerbated GVHD in WT T cell recipients, leading to decreased survival (Figure 1B). Additionally, more severe inflammatory infiltration and tissue damage in major organs were observed in mice that received anti-PD1 or anti-PDL1 (Figures 1C and 1D). In the lungs, we observed inflammatory infiltration composed of neutrophils and lymphocytes in perivascular alveolus, alveolar damage, bronchiolar epithelial hyperplasia, and detachment. In the liver, we observed portal inflammatory infiltration composed of neutrophils and lymphocytes, damaged bile duct epithelia, cytoplasmic vacuolation, and ballooning and necrosis of hepatocytes. In the intestine, mononuclear cell infiltration reached the muscle layer, with accompanying damage to the muscle tissue being observed. Other findings included necrosis of the intestinal epithelium and luminal eosinophils and villous blunting. These data are summarized in Figure 1D. Immunofluorescence staining of CD3 and PDL1 showed higher infiltration of T cells in the liver and salivary glands of mice treated with anti-PD1 or anti-PDL1 antibodies (Figure 1E). Blocking PD1 or PDL1 abrogated the protective effects otherwise conferred by $Hif1a^{-/-}$ in T cells. Thus, PDL1 is necessary for HIF1α inhibition to mediate therapeutic effects in GVHD.

We performed immunofluorescence staining of PDL1, CD3 and cleaved caspase-3 in the major organs after BMT. Strong PDL1 staining and much less donor T cell infiltration was observed for $Hif1a^{-/-}$ T cell recipients (Figure 1F). Many of the $Hif1a^{-/-}$ T cells we found in the tissues stained positive for cleaved caspase-3 (Figure 1G), which suggests that the PDL1 in these tissues induces donor T cell apoptosis to suppress GVHD.

Targeted mutation of *Hif1a* induced GVHD suppression via an HIF1α-IFN-γ-PDL1-dependent mechanism

We used flow cytometry to analyze the cellular composition of peripheral blood (PBL) and spleen from BMT recipients. Expansion of donor T cells was doubled in the spleen of $Hif1a^{-/-}$

Figure 1. Anti-PD1 and anti-PDL1 antibodies abrogate the anti-GVHD effect of targeted mutation of *Hif1a* in donor T cells

(A) Diagram of the experimental scheme. BALB/c mice received 5 × 10^6 CD45.1 T cell-depleted BM cells + 5 × 10^5 WT or $Hif1a^{-/-}$ T cells. WT and KO T cell recipients were divided to receive treatment with anti-mouse PDL1 (10F.9G2), anti-mouse PD1 (RMP1-14), or isotype control immunoglobulin G (IgG) antibodies (vehicle), as detailed in the STAR Methods.

(B) Kaplan-Meier survival curves are shown for the six groups of mice (n = 10–13 mice per group). The data are representative of three experiments.

(C) H&E-stained tissues are shown in representative images for each of six groups of mice, highlighting major pathological findings.

(D) Summary of histological scoring for the organs in each group depicted in (C). Scoring criteria are described in the STAR Methods.

(E) Representative immunofluorescence staining for CD3 and PDL1 in the liver and salivary gland (S.G.) tissues from mice receiving different treatments.

(F and G) Representative immunofluorescence images are shown for liver, lung, intestine, skin, and tongue sections from WT or $Hif1a^{-/-}$ T cell recipients. Co-staining of CD3 and PDL1 is shown in (F), and co-staining of CD3 and cleaved caspase-3 (cCasp3) is shown in (G).

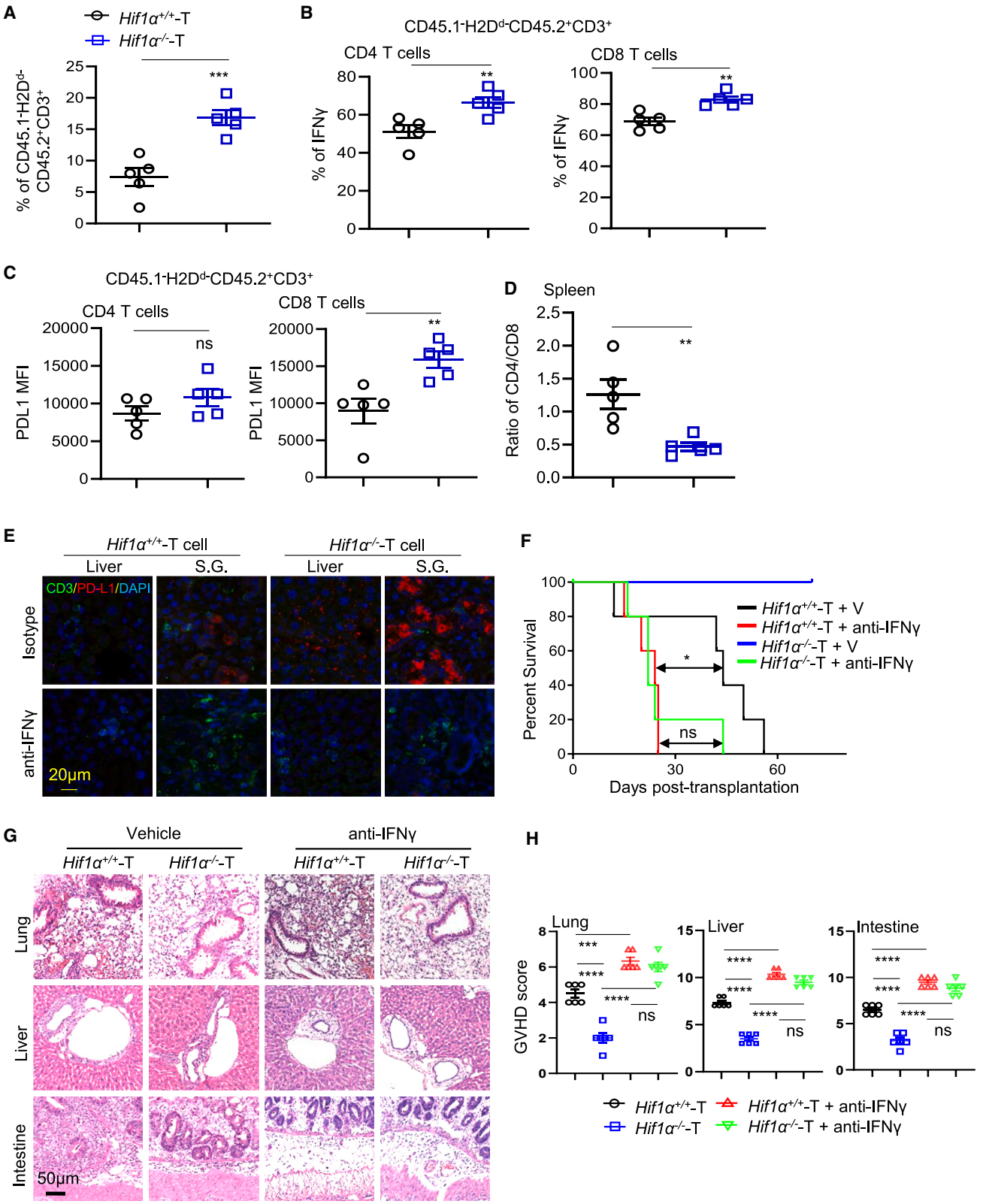

(legend on next page)

T cell recipients (Figure 2A). In the spleen, frequencies of interferon γ (IFNγ)-producing CD4 and CD8 T cells were increased in *Hif1a*$^{-/-}$ T cell recipients. In combination, the IFNγ-expressing T cells showed about 3-fold increases in the *Hif1a*$^{-/-}$ T cell recipients (Figure 2B). While a statistically significant elevation of serum IFNγ was observed in the *Hif1a*$^{-/-}$ T cell recipients (Figure S4), this increase appears marginal, presumably due to short half-lives of most cytokines. Reflecting more robust CD8 T cell activation, PDL1 was increased on splenic CD8 T cells (Figure 2C). Both WT and *Hif1a*$^{-/-}$ T cells expanded at similar rates in the PBL (Figures S5A), but we noticed a difference in the CD4/CD8 ratio in both spleen and PBL (Figures 2D and S5B). Type 1 CD8(+) T cells (Tc1) cells were increased among parent CD8 cells in the PBL for *Hif1a*$^{-/-}$ T cell recipients (Figure S5C). PDL1 was also significantly increased on CD8 T cells in PBL, with a similar (albeit not significant) trend for CD4 (Figures S5D).

To test if PDL1 is induced on host tissues in response to IFNγ produced by donor T cells, we treated BMT mice with an anti-IFNγ neutralizing monoclonal antibody (mAb), XMG1.2. Immunofluorescence showed that XMG1.2 abrogated PDL1 expression in host tissues for both WT and *Hif1a*$^{-/-}$ T cell recipients and was accompanied by increased numbers of infiltrated T cells (Figures 2E and S6). XMG1.2 accelerated the mortality rate for both recipients (Figure 2F) and resulted in more severe inflammatory infiltration and tissue damage in lung, liver, and intestines compared to control mice (Figures 2G and 2H). These data show that *Hif1a*$^{-/-}$ in donor T cells induces PDL1 expression in recipient tissues and suppresses GVHD via an Hif1α-IFNγ-PDL1-dependent mechanism.

We also analyzed CD62L and CD44 expression on gated CD4^{+} and CD8^{+} T cells from PBL of WT or *Hif1a*$^{-/-}$ donor T cell recipients. As expected, essentially all T cells from WT donor were activated; less than 1% of T cells retained the naive phenotype in PBL and less than 10% in spleen. Targeted mutation of *Hif1a* in T cells did not block T cell activation, as *Hif1a*$^{-/-}$ donor T cells also lost the naive phenotype. Nevertheless, the frequencies of central memory T cells were increased in recipients of *Hif1a*$^{-/-}$ compared with WT donor T cells (Figure S7). We noted a significant reduction of effector memory cells among the *Hif1a*$^{-/-}$ donor T cells. We also observed an increased percentage of Foxp3^{+} cells among CD4 cells from PBL, although the absolute number of regulatory T cells (Tregs) was not increased, as the total CD4 population shrank. We did not observe an increased percentage of Foxp3^{+} cells among CD4 cells in the spleen (Figure S8A).

CD8-intrinsic PDL1 can promote GVL by interacting with CD80, while host tissue-intrinsic PDL1 can attenuate GVHD by causing apoptosis and exhaustion of CD8 T cells in the target tissues by interacting with PD1.[37] As shown in Figures 2D and S4D, *Hif1a* mutation selectively increased PDL1 levels in CD8 T cells from PBL and spleen. While CD80 levels were not increased, CD80 is expressed on most CD8 T cells (Figure S8B), making it possible for a robust CD80-PDL1 interaction on *Hif1a*$^{-/-}$ CD8 T cells.

Targeting HIF1α with echinomycin suppresses GVHD via an HIF1α-IFNγ-PDL1-dependent mechanism

A recent study suggests that PDL1 on T cells may promote GVL by selective expansion of CD8 T cells, while those on host tissues may restrain GVHD.[37] It is therefore of great interest to test the effect of pharmacologically targeting HIF1α on immune cells, host tissue, and cancer cells. We established a robust xenogeneic (xeno) humanized GVHD mouse model by transplantation of human BM cells into newborn NSG pups, which developed a GVHD-like syndrome with pervasive human T cell infiltration into multiple organs, including lung, intestine, skin, kidney, liver, and stomach,[38] and avoided the weakness in the PBMC-induced adult NSG mouse model, in which the immune damage is most severe in the lung, with only mild infiltration to skin, gut, and liver.[39] To test the importance of HIF1α on therapy of GVHD induced by human cells, we examined the effect of pharmacological HIF1α inhibition on GVHD protection in the humanized GVHD mouse model. We transplanted newborn NSG pups with 0.35 × 10^{6} human BM (hBM) cells and, 10 days later, treated the recipients with 0.01 mg/kg echinomycin once every other day for 5 doses (Figure 3A). The median survival in the vehicle-treated group was 51 days compared with 99 days for the echinomycin-treated group (Figure 3B). A long-term follow up of a representative echinomycin-treated mouse is depicted in Figure S9, which shows the regrowth of hair corresponding to reduced human T cells detected in PBL throughout the experiment. In another setting, we

Figure 2. Targeted mutation of the *Hif1a* gene increased PDL1 levels in donor T cells and non-tumor host tissues via IFNγ-dependent pathway

Flow cytometry analysis of spleen samples from WT or *Hif1a*$^{-/-}$ T cell recipients 14 days after transplantation.

(A) The percentage of WT and *Hif1a*$^{-/-}$ donor T cell in splenocytes of 14 days post-transplantation mice, shown as mean ± SEM. Data are representative of 3 independent experiments.

(B) Frequency of IFNγ^{+} T cells in spleen. Splenocytes from recipients reconstituted with WT or *Hif1a*$^{-/-}$ T cells were stimulated with PMA + ionomycin for 4 h, and IFNγ expression was determined by intracellular staining. The summarized data are shown as mean ± SEM for one experiment and are representative of 3 independent experiments.

(C) The mean fluorescence intensity (MFI) of PDL1 staining is plotted for CD4 (left) and CD8 (right) donor T cells from spleens of recipient mice on day 14.

(D) The CD4/CD8 ratio of donor WT and *Hif1a*$^{-/-}$ T cells in splenocytes of 14 days post-transplantation mice was measured and summarized, shown as mean ± SEM. Data are shown for one experiment and are representative of at least 3 independent experiments.

(E) BALB/c mice received 5 × 10^{6} CD45.1 T cell-depleted BM cells + 3 × 10^{5} WT or *Hif1a*$^{-/-}$ T cells and were subsequently treated with anti-mouse IFNγ (XMG1.2) or isotype control IgG antibodies (vehicle). Representative immunofluorescence staining for CD3 and PDL1 in the liver and S.G. tissues from mice receiving different treatments.

(F) Kaplan-Meier survival curves are shown for the four groups of mice. The data are representative of three experiments.

(G) H&E-stained tissues are shown in representative images for each of four groups of mice, highlighting major pathological findings.

(H) Summary of histological scoring for the organs in each group depicted in (H). Scoring criteria are described in the STAR Methods.

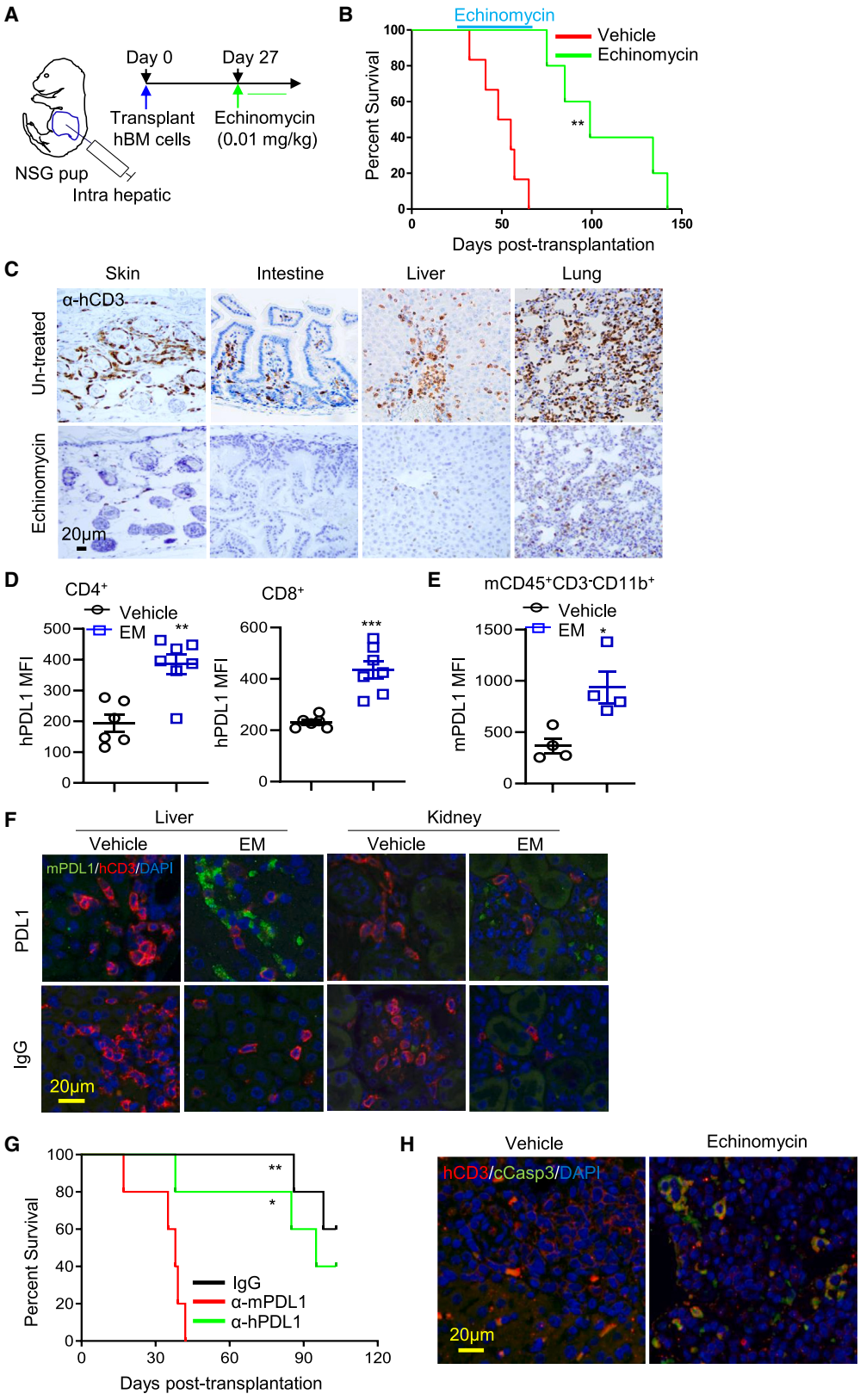

(legend on next page)

administered 5 or 20 doses of echinomycin starting on day 3 after transplantation. 100% of mice that received 20 doses of echinomycin starting this early after BMT remained alive and developed no clinical signs of GVHD throughout the entire observation period of 20 weeks, long after cessation of echinomycin treatment (Figure S10). Immunohistochemistry analysis revealed elimination of T cells from all major organs, including skin, intestine, liver, and lung (Figure 3C). We tested the expression of PDL1 in T cells. As shown in Figure 3D, PDL1 was up-regulated nearly 2-fold in the T cells by echinomycin treatment, which is consistent with the effect of genetic inactivation of *Hif1a* in mouse T cells (Figure 2C). Since PDL1 is up-regulated on host tissues in response to IFNγ produced by the CD8 T cells and is responsible for exhausting CD8 T cells in the allogeneic mouse GVHD model,[37] we tested the expression of PDL1 in the PBL of recipients after echinomycin treatment. We found significantly increased expression of human PDL1 on human T cells, and mouse PDL1 on mouse non-T cells, among PBL from recipients after echinomycin treatment (Figures 3D and 3E). The expression of mouse PDL1 was dramatically increased in the liver and kidney by echinomycin treatment (Figure 3F). To test the impact of echinomycin-induced T cell-intrinsic and -extrinsic PDL1 on GVHD, we treated the mice with anti-human or anti-mouse PDL1 mAbs. Anti-human PDL1 would not affect the function of mouse PDL1 expressed on host tissues, which may limit GVHD, whereas anti-mouse PDL1 would not affect PDL1 expressed on T cells, which may affect T cell expansion. We found that echinomycin-treated mice that received anti-mouse PDL1 antibody developed severe GVHD and died within 42 days, but the majority of mice that received echinomycin in conjunction with anti-human PDL1 survived at this time point, with 40% of the mice surviving the entire observation period (Figure 3G). Therefore, PDL1 on non-T cells conferred significant protection against GVHD. Consistent with this notion, we found that liver tissues in echinomycin-treated mice contained a high number of T cells undergoing apoptosis, while those from the vehicle-treated mice were devoid of apoptotic T cells (Figure 3H).

Targeted mutation of *Hif1a* suppressed GVHD while preserving GVL

Therapies that suppress GVHD may also suppress GVL, which is an important aspect of allo-HSCT therapeutic efficacy. To evaluate the impact of Hif1α targeting on GVL effect, we established a stable cell line with P815 mastocytoma cells expressing a luciferase reporter and monitored the tumor growth in BMT recipients using bioluminescence imaging. In this model, leukemia was induced in lethally irradiated BALB/c mice by injecting 1×10^3 luciferase-transduced P815 cells intravenously at day 0 (Figure 4A). We used bioluminescence imaging to monitor P815 cell growth *in vivo*. As shown in Figures 4B and 4C, a significantly reduced leukemia burden could be seen in recipients of P815 cells co-transplanted with WT or *Hif1a*$^{-/-}$ T cells by day 9 post-BMT, indicative of strong GVL by either T cell genotype. Recipients of P815 cells with TCD BM alone succumbed to death by leukemia by day 12 post-BMT. Co-transplantation with WT T cells prolonged the survival marginally, but the majority of these mice died of GVHD by day 14 post-BMT. In contrast, mice co-transplanted with *Hif1a*$^{-/-}$ T cells survived more than 25 days before finally dying of leukemia (Figure 4D). This demonstrates that *Hif1a* is dispensable in T cells for the preservation of GVL.

To ensure the maintenance of GVL function in *Hif1a*$^{-/-}$ T cell recipients was not unique to P815 cells, we evaluated the GVL effect of *Hif1a*$^{-/-}$ T cells on an additional line, using luciferase-transduced BCL1, a B cell leukemia/lymphoma cell line of BALB/c origin, and used bioluminescence imaging to monitor leukemia growth *in vivo* (Figures 4E and 4F). By day 7 after transplantation, recipients of WT or *Hif1a*$^{-/-}$ T cells had significantly reduced leukemia burden, indicating a strong GVL effect (Figures 4E and 4F). Consistent with GVHD data, recipients of WT T cells succumbed to GVHD by day 45 post-BMT. In contrast, most of the *Hif1a*$^{-/-}$ T cell recipients survived for more than 100 days (Figure 4G). BCL1-bearing recipients transplanted with TCD BM alone all died from progressive tumor growth by day 20 post-BMT (Figure 4G). Thus, targeted mutation

Figure 3. Echinomycin protects mice against GVHD

(A) Experimental diagram for the xeno-GVHD model. Newborn NSG pups were transplanted with 3.5×10^5 hBM cells via intrahepatic injection. 27 days after transplantation, mice were treated with 0.01 mg/kg echinomycin for a total of 20 doses. The day that mice were transplanted with hBM cells is defined as day 0. Each red arrow represents one dose of echinomycin (0.01 mg/kg, intraperitoneal injection).

(B) Kaplan-Meier survival curve is shown for the echinomycin- or vehicle-treated hBM recipients, showing significantly prolonged life span of echinomycin-treated mice.

(C) Immunohistochemistry with anti-CD3 mAb of tissues from an echinomycin-treated mouse at day 75 (bottom) and an untreated littermate that died at day 55 after transplantation with hBM (top). Data are representative of three independent experiments.

(D) Echinomycin increased the PDL1 level in donor T cells. Expression level of human PDL1 in donor T cells from hBM recipients treated with echinomycin or vehicle as described in (A), summarized as MFI of human PDL1 ± SEM analyzed by FACS. Data are representative of three independent experiments.

(E) Echinomycin increased the PDL1 level in mouse leukocytes of recipients. Expression level of mouse PDL1 in mCD45$^+$CD3$^-$CD11b$^+$ from PBL of hBM recipients treated with echinomycin or vehicle as described in (A), summarized as MFI of mouse PDL1 ± SEM. Data are representative of three independent experiments.

(F) Echinomycin increased the expression of PDL1 in liver and kidney of recipients. Recipients treated with echinomycin or vehicle as described in (A) were euthanized on day 7 after the last dose. Immunofluorescence staining with anti-human CD3 and anti-mouse PDL1 or IgG shows the increased expression of mouse PDL1 in liver and kidney of recipients treated with echinomycin compared with the vehicle-treated group. This immunofluorescence evaluation was performed in 5 mice from each group. Data are representative of three independent experiments.

(G) Kaplan-Meier survival curves of NSG recipients treated with *in vivo* anti-mouse PDL1, anti-human PDL1, and anti-mouse IgG. Data are representative of two independent experiments.

(H) Echinomycin induces apoptosis of T cells in the liver. Immunofluorescence staining of the liver tissue of recipients in with anti-human CD3 and anti-cCasp3 shows the increased apoptotic CD3$^+$ cells in echinomycin- compared with vehicle-treated mice. This immunofluorescence evaluation was performed in 5 mice from each group. Data are representative of three independent experiments.

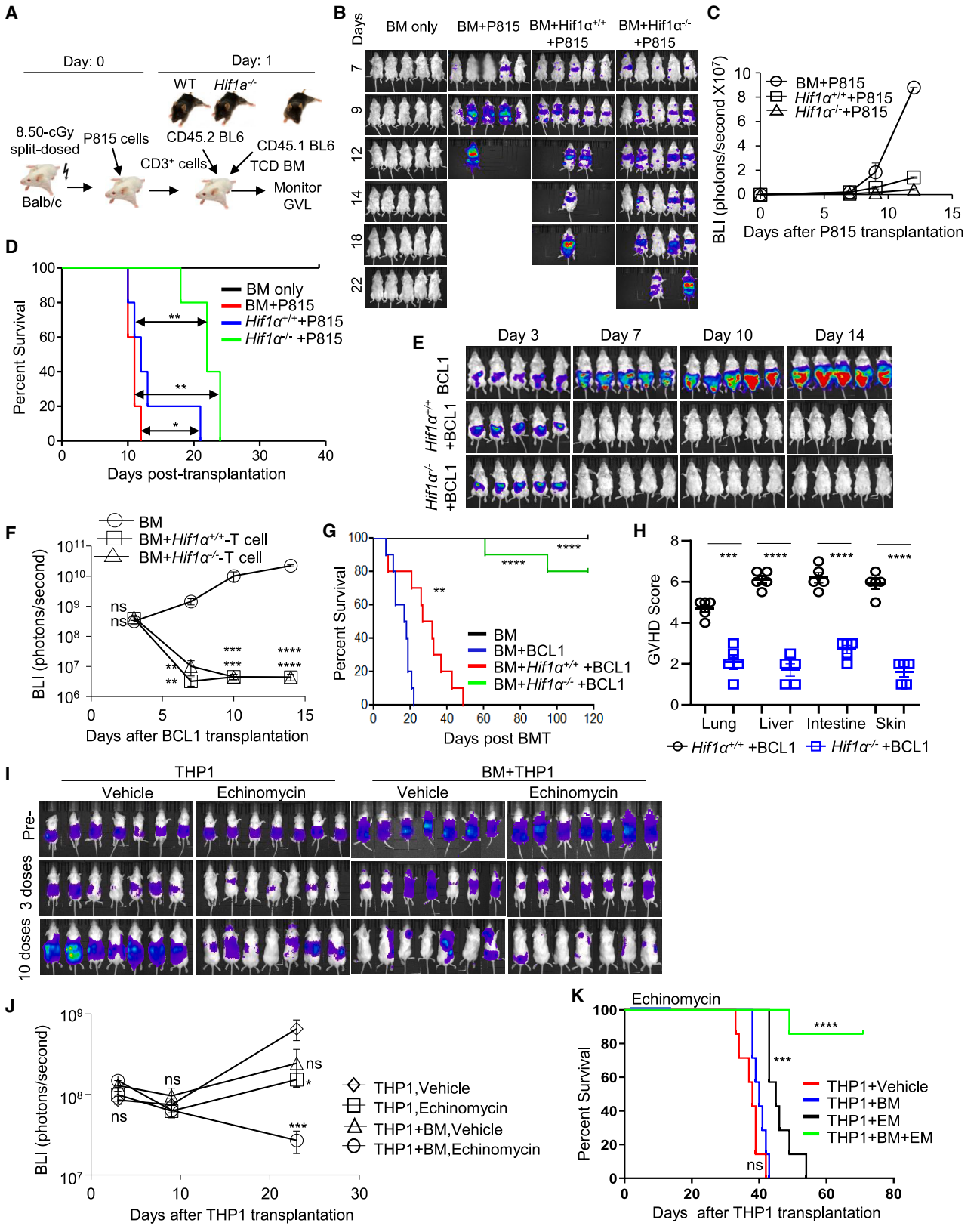

(legend on next page)

of *Hif1a* in T cells inhibits GVHD but not GVL. Further, histopathological examination of tissues such as lung, liver, intestine, and skin showed that organs from mice reconstituted with BM+BCL1+*Hif1a*$^{-/-}$ T cells had much less T cell infiltration and tissue damage than recipients reconstituted with BM+BCL1+WT T cells (Figure 4H). Although the mice reconstituted with BM+BCL1+WT T cells had significantly reduced leukemia burden compared with mice that received T-depleted BM, they died with GVHD within 50 days after BMT. These data demonstrate in a second model that *Hif1a* in T cells is dispensable for the preservation of GVL.

To test if pharmacologically targeting HIF1α could protect mice against lethal GVHD without diminishing the GVL effect, we transplanted luciferase-transduced THP1 human acute-myeloid leukemia cells, followed by hBM cells 1 day later, via intrahepatic injection into newborn NSG pups. The imaging data indicated a modest therapeutic effect of echinomycin toward THP1 leukemia cells *in vivo* (Figures 4I and 4J). THP1 growth inhibition from BMT alone was also observed but was not significant. In combination, echinomycin and BMT achieved robust reduction of leukemia and extended survival dramatically compared with the other groups (Figure 4K). Together, these data indicate that *HIF1A* in human T cells is dispensable for GVL but essential for GVHD and that the anti-leukemic effects of echinomycin may also synergize with GVL to eliminate leukemia cells.

Targeting HIF1α suppresses PDL1 expression in leukemia cells

PDL1 is a direct target gene of HIF1α,[40] and tumor cells also express HIF1α under normoxia, so we tested whether the HIF1α-PDL1 axis is also active in leukemia cells expressing HIF1α under normoxia. To test whether HIF1α inhibition is the mechanism responsible for the reduction in PDL1 protein induced by echinomycin, we used small interfering RNA (siRNA) to knock down *HIF1A* in THP1 cells (Figure 5A). We quantified PDL1 expression in THP1 with scrambled (sh-Scr) or sh-*HIF1A* by flow cytometry after a 24 h incubation with vehicle or echinomycin (Figures 5B and 5C). Under basal conditions, we found that *HIF1A* knockdown reduced PDL1 protein expression, confirming the role for *HIF1A* (Figures 5B and 5C). The inhibitory effect of echinomycin on PDL1 expression was preserved in THP1 cells transduced with scrambled short hairpin RNA (shRNA), and knockdown of *HIF1A* abrogated the ability of echinomycin to further decrease PDL1 protein (Figures 5B and 5C). These results demonstrate that HIF1α controls PDL1 expression in THP1 cells and that echinomycin reduced PDL1 by inhibiting the HIF1α-PDL1 axis. We further treated human THP1, K562, and KASUMI leukemia cell lines with 0.45 nM echinomycin in the presence or the absence of 10 ng/mL IFNγ for 24 h. Echinomycin significantly decreased expression of PDL1 in these leukemia cell lines even in the presence of IFNγ (Figure 5D). We next examined the effect of leukemia cell-intrinsic PDL1 expression on GVL in the context of HIF1α inhibition by echinomycin. We transduced THP1 cells with either empty lentiviral vector or vector containing construct for forced overexpression of PDL1. We confirmed the overexpression of PDL1 on the blasticidin-selected transduced cells by FACS (Figure 5E). We transplanted vector or PDL1 transduced THP1 cells, followed by hBM cells the following day, into newborn NSG pups by intrahepatic injection and followed the expansion of THP1 by bioluminescence imaging. The signal intensity increased sharply in the mice with PDL1-transduced THP1 cells compared to vector, indicating that forced expression of PDL1 on THP1 cells reduced GVL. The majority of mice transplanted with PDL1-transduced THP1 cells died with leukemia, whereas mice transplanted with vector-transduced THP1 cells died with GVHD (Figure 5F). The median survival of vector-THP1 recipients was 56 days as compared with 38 days for recipients of the PDL1 THP1 cells (Figure 5G), which prevented us from discerning whether PDL1 on leukemia cells may affect GVHD.

Figure 4. *Hif1a* in T cells is dispensable for GVL effect

(A–D) BALB/c mice were lethally irradiated (8.50 Gy split dosed) and inoculated with 1 × 10^3 P815-luc cells on day 0. On day 1, the mice were reconstituted with 5 × 10^6 T cell-depleted (TCD) BM (alone or mixed with 5 × 10^5 of *Hif1a* WT or *Hif1a*$^{-/-}$ purified CD3$^+$ T cells). Mice receiving TCD BM only, or TCD BM plus P815, were included as controls. P815 growth was monitored regularly using bioluminescence imaging to assess GVL.

(A) A diagram of the experimental scheme is shown.

(B) Time course of bioluminescence imaging depicted in regular imaging intervals throughout the study, showing relative P815 burden among the different groups of mice at various time points.

(C) Summarized bioluminescence intensity (BLI) data for the animals imaged on days 7 and 9.

(D) Kaplan-Meier survival curves for the mice.

(E–H) BALB/c mice were lethally irradiated (8.50 Gy split dosed) on day −1 and inoculated with 5 × 10^6 BCL1 cells 12 h later (day 0). On day 1, the mice were reconstituted with 5 × 10^6 TCD BM (alone or mixed with 5 × 10^5 of *Hif1a* WT or *Hif1a*$^{-/-}$ purified CD3$^+$ T cells).

(E) Representative images of mice are shown for the indicated time points after allo-BMT.

(F) Summarized BLI data recorded throughout the study (n = 10 mice/group).

(G) Kaplan-Meier survival curve.

(H) Summarized pathology scores for different organs are shown. The animals were euthanized on day 25 after inoculation with BCL1 cells, and the tissues were scored based on the system described in the STAR Methods.

(I) Therapeutic effect of echinomycin. 1 × 10^6 THP1 cells are delivered to mice by intrahepatic injection. Half of the mice are transplanted with 3.5 × 10^5 hBM cells via intrahepatic injection. Mice were treated with 0.01 mg/kg echinomycin or vehicle once every other day starting on day 6 for a total of 10 doses, and imaging was done on days 11 and 25. Serial imaging is shown for echinomycin- or vehicle-treated NSG recipients of THP1 or THP1 + hBM. Imaging is shown for each group on day 5, corresponding to the pretreatment values (Pre-), and on days 11 and 25, corresponding to 3 and 10 doses, respectively. Data are representative of 3 independent experiments.

(J) Quantification of BLI of mice depicted in (I). The BLI (photons/s) was measured and plotted before and after treatment and is shown as means ± SEM (n = 7 per group). Statistics are by paired Student's t test.

(K) Kaplan-Meier survival curves are shown for the mice as described in (I). Data are representative of three independent experiments.

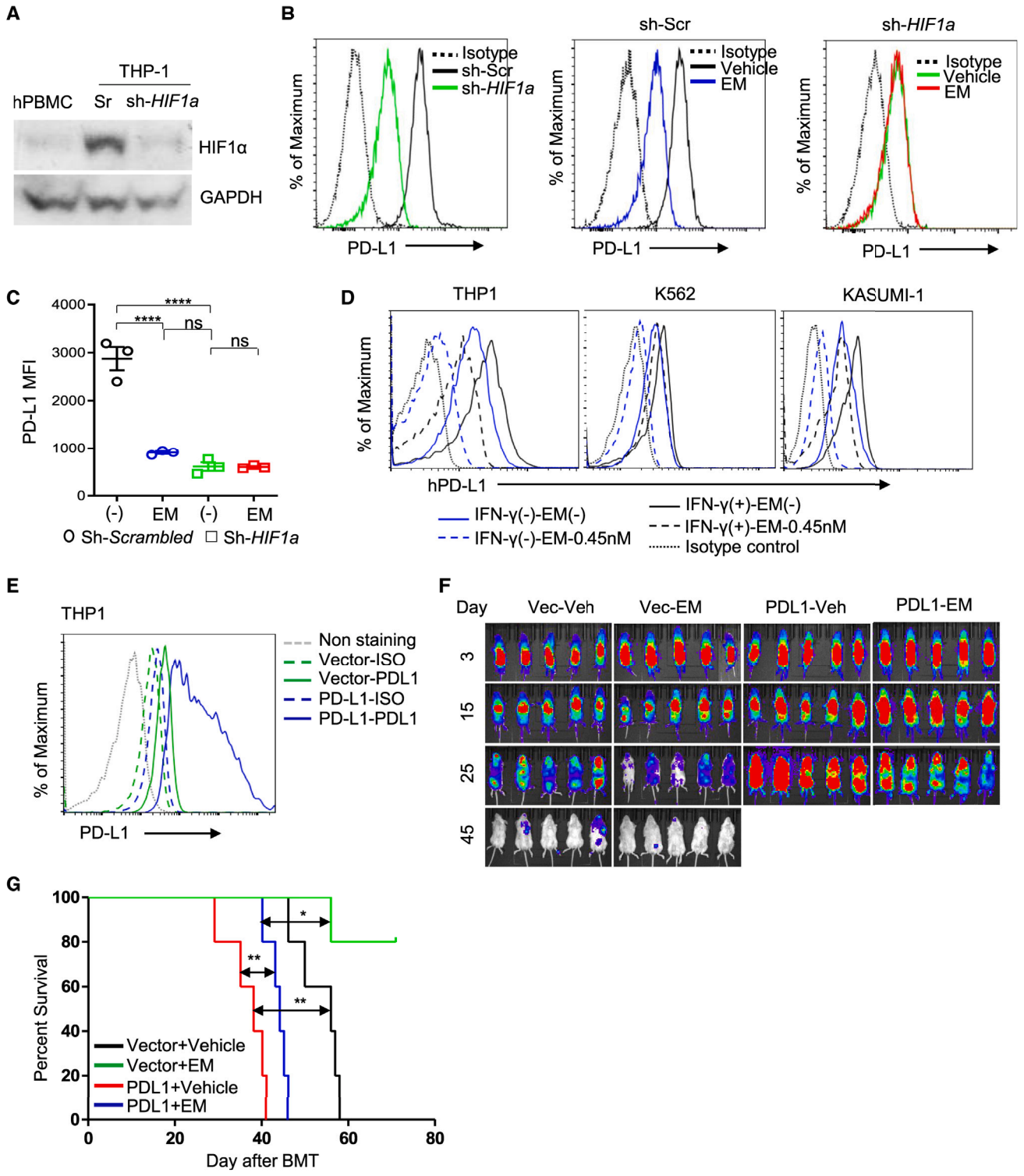

Figure 5. HIF1α drives PDL1 expression in leukemia cells

(A) Western blot HIF1α protein in THP1 cells is shown to assess the knockdown efficiency of *HIF1a* shRNA.

(B and C) Effects of *HIF1a* shRNA on PDL1 expression in THP1 cells. THP1 cells were transduced with shRNA (scrambled [sh-Scr] or *HIF1a* shRNA [sh-*HIF1a*]) and cultured under normoxia for 48 h with vehicle or echinomycin. Flow cytometry histograms depict PDL1 staining intensity comparing effects of *HIF1a* knockdown (B, left) or echinomycin between sh-Scr (B, middle) and sh-*HIF1a* (B, right) cells.

(legend continued on next page)

Similar to the results in Figure 5, echinomycin significantly prolonged the survival of mice that received vector-transduced THP1. Echinomycin still provided a survival advantage to PDL1-transduced THP1 recipients, which is consistent with its anti-leukemic effect.[30–32] The diminished protection of echinomycin against the GVL-resistant THP1-PDL1 line supports a critical function for echinomycin in enhancing GVL in this model.

Genetic and pharmaceutical inhibition of HIF1α suppresses ipilimumab-exacerbated GVHD

Having established that either genetic or pharmaceutical targeting of HIF1α can suppress GVHD, we investigated whether the efficacy of this approach can be preserved in the context of immune checkpoint blockade. Because PDL1 was found to be indispensable, we examined anti-CTLA-4 antibodies. To evaluate the effects of clinically approved anti-CTLA-4 antibodies, we took advantage of mice with knockin of the human CTLA4 gene (CTLA4$^{h/h}$), which we have previously used to study the mechanisms of irAEs with ipilimumab and other ICIs.[24,41] To allow for a comparison to be made between WT and *Hif1a*$^{-/-}$ T cell recipients, we crossed CTLA4$^{h/h}$ and *Hif1a*$^{fl/fl}$*;CD4-Cre* mice and used the T cells from Cre^{+} (*Hif1a*$^{-/-}$) or Cre^{-} (WT) littermates in the subsequent allo-BMT experiments (Figure 6A). Ipilimumab did not affect survival of the recipients of allogeneic *Hif1a*$^{-/-}$ T cells (Figure 6B), although a small increase in GVHD score was noted (Figure 6C). Echinomycin significantly prolonged survival of WT T cell recipients treated with ipilimumab (Figure 6B). Histological examination of the colon, liver, and lung showed an increase in lymphocyte infiltration, inflammation, and tissue damage in ipilimumab-treated mice (Figures 6D and 6E). Immunofluorescence staining showed that ipilimumab increased T cell infiltration in the salivary gland and liver, with only minimal effect on PDL1 (Figure 6F). Echinomycin induced PDL1 expression, while reduced ipilimumab induced T cell infiltration (Figures 6F and S11). In addition, echinomycin-treated mice showed higher levels of T cell apoptosis and a reduction in T cell proliferation in GVHD target organs (Figure S12). Taken together, the data demonstrated that genetic and pharmaceutical inhibition of HIF1α allowed use of ipilimumab in the setting of BMT.

Echinomycin potentiates anti-CTLA-4 on GVL effects

To further evaluate whether inhibition of HIF1α allowed combination of therapeutic activity of BMT and ICI, we compared mono- vs. combined effects of echinomycin and ipilimumab in a mouse model in which the allogenic T cells expressed the human *CTLA4* gene. The recipient mice were challenged with syngeneic P815 leukemia cells. While the recipients that received T cells and treatment with either ipilimumab or echinomycin alone survived longer than recipients of T cells only, survival was further prolonged by the combination of ipilimumab and echinomycin (Figures 7A and 7B).

To extend this to human T cells, we evaluated the impact of combination therapy using xenograft models consisting of hBM and leukemia cell line THP1. We transplanted luciferase-transduced THP1 cells, followed by hBM cells 1 day later, via intrahepatic injection into newborn NSG pups, as described in Figure 4A. Mice were imaged on day 7 after receiving THP1 cells. Ipilimumab alone reduced THP1 burden compared to vehicle-treated mice, although no mice were cured before they died with GVHD (Figures 7C and 7D). Echinomycin alone marginally reduced THP1 leukemia cells *in vivo*, although a significant impact on survival was observed, presumably due to the curative effect of GVHD. Elimination of leukemia cells and mortality of recipient mice were achieved only in mice treated with both echinomycin and ipilimumab (Figures 7C and 7D). Taken together, data in Figure 7 demonstrated that echinomycin allowed combination of BMT with anti-CTLA-4 immunotherapy.

DISCUSSION

Despite major advances in multiple types of malignancies, administration of ICI after, or as a bridge to BMT, carries the significant risk of exaggerating GVHD.[12–16] Here, we showed that both PD(L)1 and CTLA-4 immune checkpoints can be targeted in the BMT setting: CTLA-4 is targeted by anti-CTLA-4 mAb ipilimumab, while PDL1 on the leukemia cells is targeted by using an HIF1α inhibitor. More importantly, targeting HIF1α suppresses ipilimumab-exacerbated GVHD in the context of BMT.

HIF1α has been shown to play a critical role in driving T cell differentiation, metabolism, and cytotoxic activity.[42–44] T cell activation both induces and stabilizes HIF1α, leading to increased cytolytic activity of CD8^{+} T cells.[43–45] Here, we showed that human T cells expanded in BMT express high levels of HIF1α. The impact of T cell-intrinsic targeted mutation of *Hif1a* on GVHD is demonstrated by the data that targeted mutation of *Hif1a* in donor T cells prevented GVHD and significantly reduced mortality in allogeneic recipient mice, even in combination with ipilimumab. The lack of GVHD was not due to failure in T cell expansion, as a high frequency of *Hif1a*$^{-/-}$ donor T cells was observed in the recipient mice. Interestingly, relative to WT donor cells, the *Hif1a*$^{-/-}$ donor T cells experienced

(C) The data are summarized, expressed as mean ± SEM of PDL1 MFI for triplicate wells, and were analyzed by one-way ANOVA with Sidak's post hoc test. Data are representative of 3 independent experiments.

(D) Reduced PDL1 protein levels on human leukemia cell lines treated with echinomycin, with or without IFNγ. THP1, K562, and KASUMI cell lines were treated with 0.45 nM echinomycin with or without IFN-γ (10 ng/mL) for 24 h prior to flow cytometry.

(E–G) Forced expression of PDL1 on THP1 cells inhibits GVL. THP1 cells were infected with lentivirus containing construct for PDL1 overexpression or vector. The infected THP1 cells were selected by blasticidin and stained with anti-PDL1 antibody. PDL1 overexpression in the selected THP1 cells is shown by FACS analysis (E). Newborn pups were transplanted by intrahepatic injection with the blasticidin-selected THP1 cells expressing vector or PDL1 overexpression construct, followed by 3.5 × 10^{5} hBM cells the next day. Mice were treated with 0.01 mg/kg echinomycin or vehicle every other day for 10 doses starting on day 3. Serial imaging was performed for echinomycin- or vehicle-treated NSG recipients by bioluminescence imaging. Imaging is shown for each group on day 3, corresponding to the pretreatment values, and on days 15, 25, and 45 after BMT (F). Kaplan-Meier survival curve is shown for the echinomycin- or vehicle-treated hBM recipients (G). Data are representative of two independent experiments.

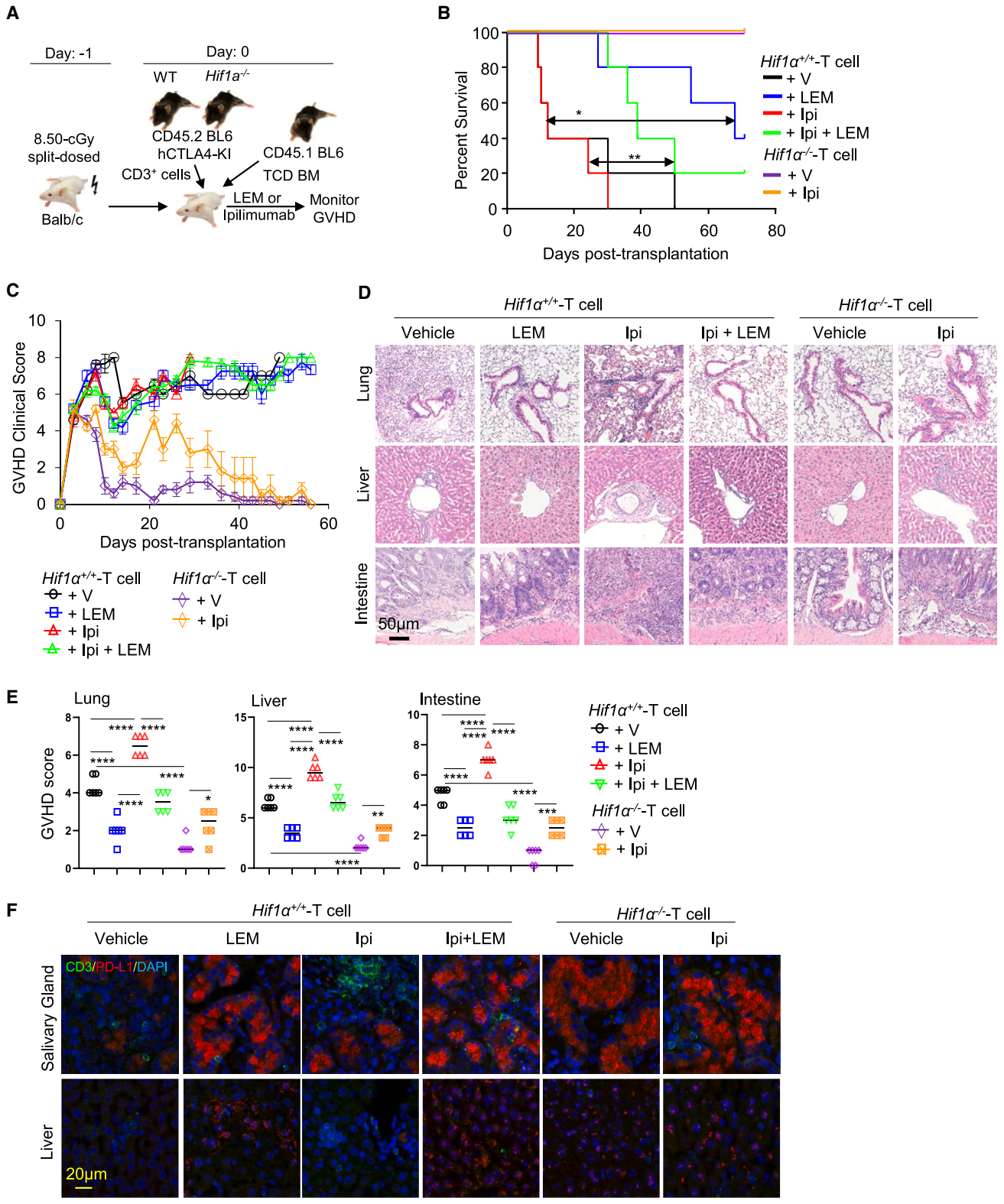

Figure 6. Targeting HIF1α reduced CTLA-4 antibody-accelerated GVHD

(A) Diagram of the experimental scheme. Lethally irradiated (8.50-Gy split dosed) BALB/c mice were rescued with 5 × 10^6 TCD BM cells from CD45.1 mice, spiked with either 5 × 10^5 WT or *Hif1a*$^{-/-}$ purified CD3$^+$ T cells from a CD45.2 background with knockin of the human *CTLA4* gene (CTLA4$^{h/h}$). Mice that received

(legend continued on next page)

preferential expansion of CD8 T cells, resulting in a dramatically reduced CD4/CD8 T cell ratio. The preferential expansion of CD8 T cells is relevant to human allo-HSCT, as recent studies demonstrated that the ratio of CD4/CD8 is lower in non-GVHD patients compared with in patients with GVHD in the clinic,[46] and the low CD4/CD8 ratio is a good predictor for relapse-free survival.[47] This notion is consistent with several preclinical studies that showed that depletion of CD4 T cells early after allo-HSCT preserves GVL while attenuating GVHD[37] and that CD8 T cells prevent GVHD while mediating GVL.[48,49]

PD1 negatively regulates T cell immune function through the interaction with its ligand PDL1. PDL1 is expressed on both hematopoietic and non-hematopoietic cells, and the expression can be induced by immune stimulation.[50,51] Accumulating data suggest multiple functions of PDL1 in the setting of BMT for patients with leukemia. Thus, PDL1 expression on parenchymal cells is critical for suppression of acute GVHD,[52] as PD1/PDL1 blockade with mAbs exacerbates acute GVHD.[25,52] On the other hand, CD8-intrinsic PDL1 can promote GVL through its interaction with CD80, while host tissue-intrinsic PDL1 can induce CD8 T cell apoptosis and exhaustion in target tissues to reduce GVHD.[37] The cell-type-specific function with the opposite consequence for host survival made it difficult to use a conventional approach to target PDL1 in the BMT setting. Our data presented in this study demonstrated that targeting HIF1α offered a superior approach, as it can selectively abrogate immune evasion by PDL1 while preserving and enhancing the beneficial effect of PDL1 in the BMT setting.

It was shown that microRNA-31 regulates T cell metabolism via HIF1α and promotes chronic GVHD pathogenesis in mice.[53] This finding complements our data on acute GVHD models. The outcomes of HIF1α deletion in T cells are superior to that of treatment with echinomycin as manifested by the fact T cell-selective knockout (KO) of Hif1α was sufficient to eliminate mortality from GVHD in this study. Pharmacokinetic limitations of drug treatment are the most likely explanation for the inferior effect of echinomycin, although a counter effect of echinomycin on non-T host cells cannot be ruled out.

Our observation that HIF1α promotes PDL1 expression in leukemia cells is consistent with prior work demonstrating transcriptional activation of PDL1 by *HIF1a*.[40,54] How *HIF1a* suppress PDL1 expression in T cells and host tissues requires further studies. Our results suggest that T cell-intrinsic HIF1α inhibits PDL1 expression on T cells indirectly by suppressing IFNγ production in the setting of GVHD and/or ipilimumab treatment.

Concomitant targeting of both CTLA-4 and PD(L)1 remains the most effective immunotherapy for cancer, although its adoption has been limited due to toxicity. Such an approach has not been widely attempted in BMT, presumably because of the exacerbation of toxicity associated GVHD.[21] Our recent study demonstrated that combining an HIF1α inhibitor with anti-CTLA-4 mAbs can reduce toxicity associated with co-targeting of PD(L)1 and CTLA-4 in tumor-bearing mice.[24] Here, we report that by inducing PDL1 in host organs, the HIF1α inhibitor allowed adoption of anti-CTLA-4 mAbs in the BMT setting, resulting in elimination of both leukemia and mortality in the mouse model comprising hBM and leukemia cells. Our finding has the potential to improve the survival of patients with leukemia by allowing combination of GVL and ICI, two curative treatments for hematological malignancies.

Limitations of the study

This study utilized acute GVHD mouse models, limiting the generalizability of the findings to chronic GVHD. The impact of HIF1α inhibition on chronic GVHD was not explored in this research. The potential role of HIF1α in regulating B cell functions within the context of chronic GVHD remains unaddressed. Further examination of HIF1α's role across various GVHD scenarios will broaden the clinical relevance of the findings in the context of allo-HSCT combined with ICIs.

STAR★METHODS

Detailed methods are provided in the online version of this paper and include the following:

- KEY RESOURCES TABLE
- RESOURCE AVAILABILITY
  - Lead contact
  - Materials availability
  - Data and code availability
- EXPERIMENTAL MODEL AND STUDY PARTICIPANT DETAILS
  - Mice
- METHOD DETAILS
  - Allogeneic mouse model of GVHD and GVL
  - Xenogeneic GVHD and GVL model
  - Gene set enrichment analysis (GSEA)
  - Gene transcript analysis of patient samples
  - Flow cytometry
  - Immunofluorescence staining
  - Pathology scores
  - Clinical GVHD assessment
  - Bioluminescence imaging
- QUANTIFICATION AND STATISTICAL ANALYSIS

Hif1a WT T cells were split into 4 groups to receive treatment with vehicle control, liposomal echinomycin (LEM) (0.05 mg/kg, intravenously [i.v.]), ipilimumab (0.2 mg, intraperitoneally [i.p.]), or a combination of liposomal echinomycin and ipilimumab, and the mice that received *Hif1a*$^{-/-}$ T cells received vehicle control or 0.2 mg ipilimumab. All treatments were given on days 3, 5, and 7. The mice were observed regularly to assess GVHD and determine mortality rate.

(B) Kaplan-Meier survival curve is shown for the mice receiving different T cell genotypes and treatments.

(C) Clinical GVHD scores are shown for recipients of WT or *Hif1a*$^{-/-}$ donor T cells that receive treatment. The mice were scored as described in Figure 1D and are shown as means ± SEM.

(D) Representative images of H&E-stained tissues in the lung, liver, and colon of the mice.

(E) Summarized pathology scores in the tissues depicted in (D).

(F) Representative immunofluorescence staining of CD3 and PDL1 in the S.G. and liver tissues from the mice receiving different T cell genotypes and treatments.

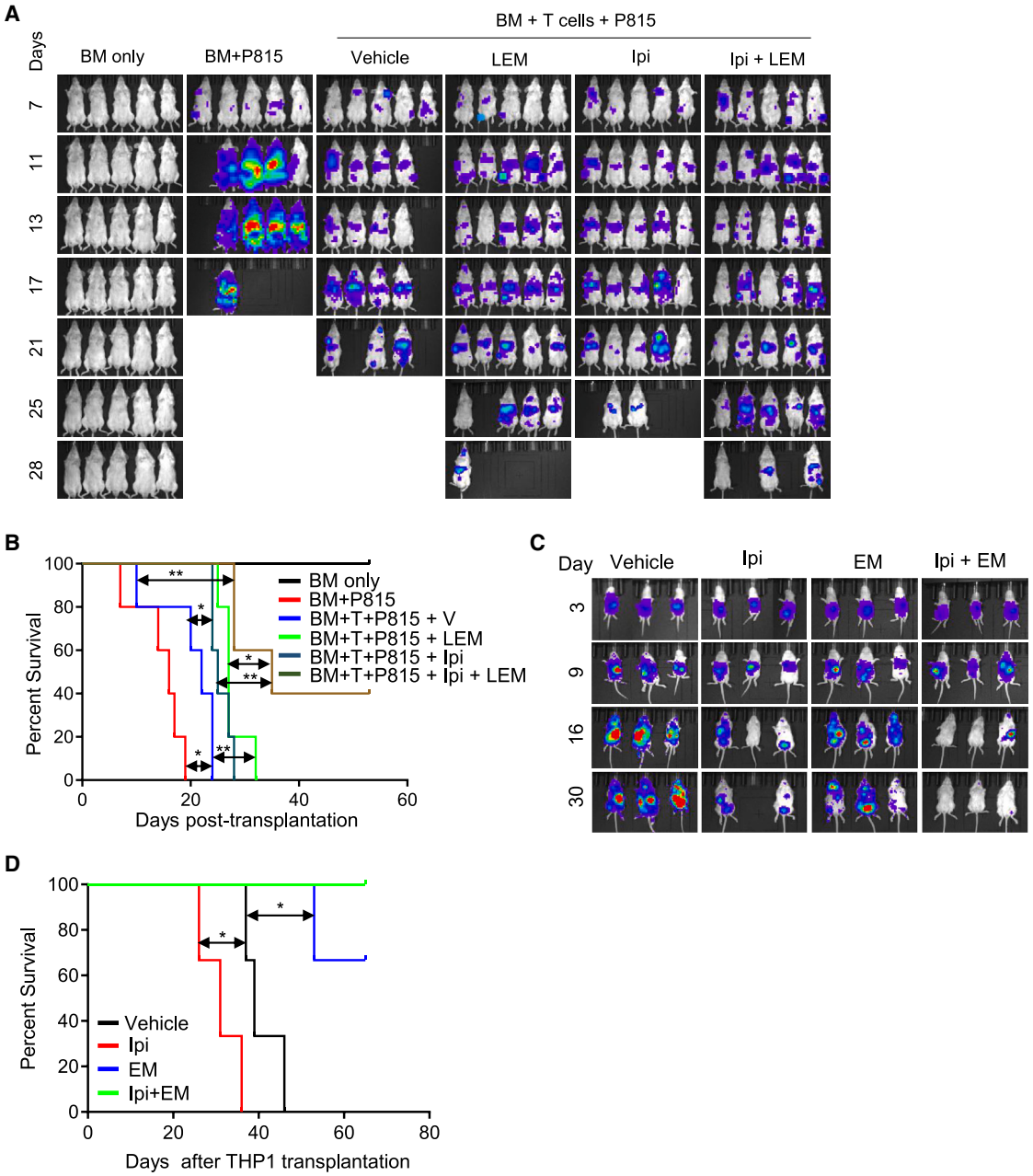

Figure 7. Echinomycin in combination with ipilimumab prolonged the life span of tumor-bearing mice after BMT

(A and B) BALB/c mice were lethally irradiated (8.50 Gy split dosed) and inoculated with 1 × 10^3 P815-luc cells on day 0. On day 1, the mice were reconstituted with 5 × 10^6 TCD BM cells from CD45.1 mice, spiked with 5 × 10^5 of WT or *Hif1a*$^{-/-}$purified CD3$^+$ T cells from a CD45.2 background with knockin of the human *CTLA4* gene (CTLA4$^{h/h}$). Mice that received *Hif1a* WT T cells were split into six groups to receive treatment with vehicle control, liposomal echinomycin (0.05 mg/kg, i.v.), ipilimumab (0.2 mg, i.p.), or a combination of liposomal echinomycin and ipilimumab. All treatments were given on days 3, 5, and 7. The mice were observed regularly to assess GVHD and determine mortality rate.

(A) Time course of bioluminescence imaging depicted in regular imaging intervals throughout the study, showing relative P815 burden among the different groups of mice at various time points.

(B) Kaplan-Meier survival curve is shown for the mice receiving different treatments.

(C and D) Newborn pups were transplanted by intrahepatic injection with 1 × 10^6 of THP1 cells at day 0, followed by 4.5 × 10^5 hBM cells the next day. Mice were treated with echinomycin (0.01 mg/kg, i.p.), ipilimumab (0.2 mg, i.p.), or a combination of echinomycin and ipilimumab. Ipilimumab treatments were given on days 3, 5, and 7. Echinomycin treatments were given on days 3, 5, 7, 9, and 11.

(C) Serial imaging was performed for the treated NSG recipients by bioluminescence imaging. Imaging is shown for each group on day 3, corresponding to the pretreatment values, and on days 9, 16, and 30 after BMT.

(D) Kaplan-Meier survival curve is shown for the different treatment tumor-bearing recipients. Data are representative of two independent experiments.

SUPPLEMENTAL INFORMATION

Supplemental information can be found online at https://doi.org/10.1016/j.xcrm.2023.101236.

ACKNOWLEDGMENTS

Funding was provided by the NIH (grants CA219150 and CA227671 to Y.W. and CA171972 and CA183030 to Y.L.). Parts of the studies were performed when the authors were at the Children's National Medical Center at Washington DC.

AUTHOR CONTRIBUTIONS

C.B., Yan Liu, and Y. Wang. designed and performed research and also prepared the manuscript. J.Y., D.H., and C.Q. collected patient materials and performed qPCR analysis. Y. Wei performed histological experiments. Peng Zhang performed bioinformatics analyses. C.L. sorted cells. J.S., F.T., C.-s.W., and Pan Zheng provided advice on experimental design and helped with flow cytometry, histological experiments, and the interpretation of the results. Y. Wang., Yang Liu, and Yan Liu designed the study, analyzed data, supervised the study, and wrote the manuscript.

DECLARATION OF INTERESTS

Yang Liu and Pan Zheng are among the co-founders of and have equity interest in OncoC4, Inc.

INCLUSION AND DIVERSITY

We support inclusive, diverse, and equitable conduct of research.

Received: April 17, 2023
Revised: July 27, 2023
Accepted: September 20, 2023
Published: October 11, 2023

REFERENCES

1. Thomas, E.D., Lochte, H.L., Jr., Lu, W.C., and Ferrebee, J.W. (1957). Intravenous infusion of bone marrow in patients receiving radiation and chemotherapy. N. Engl. J. Med. *257*, 491–496. https://doi.org/10.1056/NEJM195709122571102.
2. Thanarajasingam, G., Kim, H.T., Cutler, C., Ho, V.T., Koreth, J., Alyea, E.P., Antin, J.H., Soiffer, R.J., and Armand, P. (2013). Outcome and prognostic factors for patients who relapse after allogeneic hematopoietic stem cell transplantation. Biol. Blood Marrow Transplant. *19*, 1713–1718. https://doi.org/10.1016/j.bbmt.2013.09.011.
3. Zuanelli Brambilla, C., Lobaugh, S.M., Ruiz, J.D., Dahi, P.B., Goldberg, A.D., Young, J.W., Gyurkocza, B., Shaffer, B.C., Ponce, D.M., Tamari, R., et al. (2021). Relapse after Allogeneic Stem Cell Transplantation of Acute Myelogenous Leukemia and Myelodysplastic Syndrome and the Importance of Second Cellular Therapy. Transplant. Cell. Ther. *27*, 771.e1–771.e10. https://doi.org/10.1016/j.jtct.2021.05.011.
4. Mielcarek, M., Storer, B.E., Flowers, M.E.D., Storb, R., Sandmaier, B.M., and Martin, P.J. (2007). Outcomes among patients with recurrent high-risk hematologic malignancies after allogeneic hematopoietic cell transplantation. Biol. Blood Marrow Transplant. *13*, 1160–1168. https://doi.org/10.1016/j.bbmt.2007.06.007.
5. Ferrara, J.L.M., Levine, J.E., Reddy, P., and Holler, E. (2009). Graft-versus-host disease. Lancet *373*, 1550–1561. https://doi.org/10.1016/S0140-6736(09)60237-3.
6. Jacobsohn, D.A., and Vogelsang, G.B. (2007). Acute graft versus host disease. Orphanet J. Rare Dis. *2*, 35. https://doi.org/10.1186/1750-1172-2-35.
7. Copelan, E.A. (2006). Hematopoietic stem-cell transplantation. N. Engl. J. Med. *354*, 1813–1826. https://doi.org/10.1056/NEJMra052638.
8. Strome, S.E., Dong, H., Tamura, H., Voss, S.G., Flies, D.B., Tamada, K., Salomao, D., Cheville, J., Hirano, F., Lin, W., et al. (2003). B7-H1 blockade augments adoptive T-cell immunotherapy for squamous cell carcinoma. Cancer Res. *63*, 6501–6505.
9. Iwai, Y., Ishida, M., Tanaka, Y., Okazaki, T., Honjo, T., and Minato, N. (2002). Involvement of PD-L1 on tumor cells in the escape from host immune system and tumor immunotherapy by PD-L1 blockade. Proc. Natl. Acad. Sci. USA *99*, 12293–12297. https://doi.org/10.1073/pnas.192461099.
10. Dong, H., Strome, S.E., Salomao, D.R., Tamura, H., Hirano, F., Flies, D.B., Roche, P.C., Lu, J., Zhu, G., Tamada, K., et al. (2002). Tumor-associated B7-H1 promotes T-cell apoptosis: a potential mechanism of immune evasion. Nat. Med. *8*, 793–800. https://doi.org/10.1038/nm730.
11. Sanmamed, M.F., and Chen, L. (2019). A Paradigm Shift in Cancer Immunotherapy: From Enhancement to Normalization. Cell *176*, 677. https://doi.org/10.1016/j.cell.2019.01.008.
12. Davids, M.S., Kim, H.T., Bachireddy, P., Costello, C., Liguori, R., Savell, A., Lukez, A.P., Avigan, D., Chen, Y.B., McSweeney, P., et al. (2016). Ipilimumab for Patients with Relapse after Allogeneic Transplantation. N. Engl. J. Med. *375*, 143–153. https://doi.org/10.1056/NEJMoa1601202.
13. Armand, P., Shipp, M.A., Ribrag, V., Michot, J.M., Zinzani, P.L., Kuruvilla, J., Snyder, E.S., Ricart, A.D., Balakumaran, A., Rose, S., and Moskowitz, C.H. (2016). Programmed Death-1 Blockade With Pembrolizumab in Patients With Classical Hodgkin Lymphoma After Brentuximab Vedotin Failure. J. Clin. Oncol. *34*, 3733–3739. https://doi.org/10.1200/JCO.2016.67.3467.
14. Younes, A., Santoro, A., Shipp, M., Zinzani, P.L., Timmerman, J.M., Ansell, S., Armand, P., Fanale, M., Ratanatharathorn, V., Kuruvilla, J., et al. (2016). Nivolumab for classical Hodgkin's lymphoma after failure of both autologous stem-cell transplantation and brentuximab vedotin: a multicentre, multicohort, single-arm phase 2 trial. Lancet Oncol. *17*, 1283–1294. https://doi.org/10.1016/S1470-2045(16)30167-X.
15. Beköz, H., Karadurmuş, N., Paydaş, S., Türker, A., Toptaş, T., Fıratlı Tuğlular, T., Sönmez, M., Gülbaş, Z., Tekgündüz, E., Kaya, A.H., et al. (2017). Nivolumab for relapsed or refractory Hodgkin lymphoma: real-life experience. Ann. Oncol. *28*, 2496–2502. https://doi.org/10.1093/annonc/mdx341.
16. Merryman, R.W., Castagna, L., Giordano, L., Ho, V.T., Corradini, P., Guidetti, A., Casadei, B., Bond, D.A., Jaglowski, S., Spinner, M.A., et al. (2021). Allogeneic transplantation after PD-1 blockade for classic Hodgkin lymphoma. Leukemia *35*, 2672–2683. https://doi.org/10.1038/s41375-021-01193-6.
17. Ijaz, A., Khan, A.Y., Malik, S.U., Faridi, W., Fraz, M.A., Usman, M., Tariq, M.J., Durer, S., Durer, C., Russ, A., et al. (2019). Significant Risk of Graft-versus-Host Disease with Exposure to Checkpoint Inhibitors before and after Allogeneic Transplantation. Biol. Blood Marrow Transplant. *25*, 94–99. https://doi.org/10.1016/j.bbmt.2018.08.028.
18. Herbaux, C., Gauthier, J., Brice, P., Drumez, E., Ysebaert, L., Doyen, H., Fornecker, L., Bouabdallah, K., Manson, G., Ghesquières, H., et al. (2017). Efficacy and tolerability of nivolumab after allogeneic transplantation for relapsed Hodgkin lymphoma. Blood *129*, 2471–2478. https://doi.org/10.1182/blood-2016-11-749556.
19. Chen, R., Zinzani, P.L., Lee, H.J., Armand, P., Johnson, N.A., Brice, P., Radford, J., Ribrag, V., Molin, D., Vassilakopoulos, T.P., et al. (2019). Pembrolizumab in relapsed or refractory Hodgkin lymphoma: 2-year follow-up of KEYNOTE-087. Blood *134*, 1144–1153. https://doi.org/10.1182/blood.2019000324.
20. Meti, N., Esfahani, K., and Johnson, N.A. (2018). The Role of Immune Checkpoint Inhibitors in Classical Hodgkin Lymphoma. Cancers *10*, 204. https://doi.org/10.3390/cancers10060204.
21. Merryman, R.W., Kim, H.T., Zinzani, P.L., Carlo-Stella, C., Ansell, S.M., Perales, M.A., Avigdor, A., Halwani, A.S., Houot, R., Marchand, T., et al.

(2017). Safety and efficacy of allogeneic hematopoietic stem cell transplant after PD-1 blockade in relapsed/refractory lymphoma. Blood *129*, 1380–1388. https://doi.org/10.1182/blood-2016-09-738385.

22. Haverkos, B.M., Abbott, D., Hamadani, M., Armand, P., Flowers, M.E., Merryman, R., Kamdar, M., Kanate, A.S., Saad, A., Mehta, A., et al. (2017). PD-1 blockade for relapsed lymphoma post-allogeneic hematopoietic cell transplant: high response rate but frequent GVHD. Blood *130*, 221–228. https://doi.org/10.1182/blood-2017-01-761346.

23. Kasamon, Y.L., de Claro, R.A., Wang, Y., Shen, Y.L., Farrell, A.T., and Pazdur, R. (2017). FDA Approval Summary: Nivolumab for the Treatment of Relapsed or Progressive Classical Hodgkin Lymphoma. Oncol. *22*, 585–591. https://doi.org/10.1634/theoncologist.2017-0004.

24. Bailey, C.M., Liu, Y., Liu, M., Du, X., Devenport, M., Zheng, P., Liu, Y., and Wang, Y. (2022). Targeting HIF-1alpha abrogates PD-L1-mediated immune evasion in tumor microenvironment but promotes tolerance in normal tissues. J. Clin. Invest. *132*, e150846. https://doi.org/10.1172/JCI150846.

25. Blazar, B.R., Carreno, B.M., Panoskaltsis-Mortari, A., Carter, L., Iwai, Y., Yagita, H., Nishimura, H., and Taylor, P.A. (2003). Blockade of programmed death-1 engagement accelerates graft-versus-host disease lethality by an IFN-gamma-dependent mechanism. J. Immunol. *171*, 1272–1277. https://doi.org/10.4049/jimmunol.171.3.1272.

26. Furlan, S.N., Watkins, B., Tkachev, V., Flynn, R., Cooley, S., Ramakrishnan, S., Singh, K., Giver, C., Hamby, K., Stempora, L., et al. (2015). Transcriptome analysis of GVHD reveals aurora kinase A as a targetable pathway for disease prevention. Sci. Transl. Med. *7*, 315ra191. https://doi.org/10.1126/scitranslmed.aad3231.

27. Semenza, G.L. (2003). Targeting HIF-1 for cancer therapy. Nat. Rev. Cancer *3*, 721–732. https://doi.org/10.1038/nrc1187.

28. Semenza, G.L. (2001). HIF-1, O(2), and the 3 PHDs: how animal cells signal hypoxia to the nucleus. Cell *107*, 1–3.

29. Hong, S.S., Lee, H., and Kim, K.W. (2004). HIF-1alpha: a valid therapeutic target for tumor therapy. Cancer Res. Treat. *36*, 343–353. https://doi.org/10.4143/crt.2004.36.6.343.

30. Wang, Y., Liu, Y., Malek, S.N., Zheng, P., and Liu, Y. (2011). Targeting HIF1alpha eliminates cancer stem cells in hematological malignancies. Cell Stem Cell *8*, 399–411. https://doi.org/10.1016/j.stem.2011.02.006.

31. Wang, Y., Liu, Y., Tang, F., Bernot, K.M., Schore, R., Marcucci, G., Caligiuri, M.A., Zheng, P., and Liu, Y. (2014). Echinomycin protects mice against relapsed acute myeloid leukemia without adverse effect on hematopoietic stem cells. Blood *124*, 1127–1135. https://doi.org/10.1182/blood-2013-12-544221.

32. Wang, Y., Liu, Y., Bailey, C., Zhang, H., He, M., Sun, D., Zhang, P., Parkin, B., Baer, M.R., Zheng, P., et al. (2020). Therapeutic targeting of TP53-mutated acute myeloid leukemia by inhibiting HIF-1alpha with echinomycin. Oncogene *39*, 3015–3027. https://doi.org/10.1038/s41388-020-1201-z.

33. Bailey, C.M., Liu, Y., Peng, G., Zhang, H., He, M., Sun, D., Zheng, P., Liu, Y., and Wang, Y. (2020). Liposomal formulation of HIF-1alpha inhibitor echinomycin eliminates established metastases of triple-negative breast cancer. Nanomedicine *29*, 102278. https://doi.org/10.1016/j.nano.2020.102278.

34. Liu, Y., Nelson, M.V., Bailey, C., Zhang, P., Zheng, P., Dome, J.S., Liu, Y., and Wang, Y. (2021). Targeting the HIF-1alpha-IGFBP2 axis therapeutically reduces IGF1-AKT signaling and blocks the growth and metastasis of relapsed anaplastic Wilms tumor. Oncogene *40*, 4809–4819. https://doi.org/10.1038/s41388-021-01907-1.

35. Peng, G., Wang, Y., Ge, P., Bailey, C., Zhang, P., Zhang, D., Meng, Z., Qi, C., Chen, Q., Chen, J., et al. (2021). The HIF1alpha-PDGFD-PDGFRalpha axis controls glioblastoma growth at normoxia/mild-hypoxia and confers sensitivity to targeted therapy by echinomycin. J. Exp. Clin. Cancer Res. *40*, 278. https://doi.org/10.1186/s13046-021-02082-7.

36. Hsiao, M., Tatishchev, S., Khedro, T., Yaghmour, B., O'Connell, C., and Yaghmour, G. (2020). First Report of Severe Acute Graft-Versus-Host Disease After Allogeneic Stem Cell Transplant in a Patient With Myelodysplastic Syndrome Treated With Atezolizumab: Literature Review. World J. Oncol. *11*, 112–115. https://doi.org/10.14740/wjon1263.

37. Ni, X., Song, Q., Cassady, K., Deng, R., Jin, H., Zhang, M., Dong, H., Forman, S., Martin, P.J., Chen, Y.Z., et al. (2017). PD-L1 interacts with CD80 to regulate graft-versus-leukemia activity of donor CD8+ T cells. J. Clin. Invest. *127*, 1960–1977. https://doi.org/10.1172/JCI91138.

38. Liu, Y., Bailey, C., Lazarski, C., Wong, C.-s., Zheng, P., Liu, Y., and Wang, Y. (2017). Treatment of Graft-versus-Host Disease by Echinomycin in a New Humanized Mouse Model. Preprint at bioRxiv. https://doi.org/10.1101/108951.

39. Covassin, L., Laning, J., Abdi, R., Langevin, D.L., Phillips, N.E., Shultz, L.D., and Brehm, M.A. (2011). Human peripheral blood CD4 T cell-engrafted non-obese diabetic-scid IL2rgamma(null) H2-Ab1 (tm1Gru) Tg (human leucocyte antigen D-related 4) mice: a mouse model of human allogeneic graft-versus-host disease. Clin. Exp. Immunol. *166*, 269–280. https://doi.org/10.1111/j.1365-2249.2011.04462.x.

40. Barsoum, I.B., Smallwood, C.A., Siemens, D.R., and Graham, C.H. (2014). A mechanism of hypoxia-mediated escape from adaptive immunity in cancer cells. Cancer Res. *74*, 665–674. https://doi.org/10.1158/0008-5472.CAN-13-0992.

41. Du, X., Liu, M., Su, J., Zhang, P., Tang, F., Ye, P., Devenport, M., Wang, X., Zhang, Y., Liu, Y., and Zheng, P. (2018). Uncoupling therapeutic from immunotherapy-related adverse effects for safer and effective anti-CTLA-4 antibodies in CTLA4 humanized mice. Cell Res. *28*, 433–447. https://doi.org/10.1038/s41422-018-0012-z.

42. Palazon, A., Goldrath, A.W., Nizet, V., and Johnson, R.S. (2014). HIF transcription factors, inflammation, and immunity. Immunity *41*, 518–528. https://doi.org/10.1016/j.immuni.2014.09.008.

43. Doedens, A.L., Phan, A.T., Stradner, M.H., Fujimoto, J.K., Nguyen, J.V., Yang, E., Johnson, R.S., and Goldrath, A.W. (2013). Hypoxia-inducible factors enhance the effector responses of CD8(+) T cells to persistent antigen. Nat. Immunol. *14*, 1173–1182. https://doi.org/10.1038/ni.2714.

44. Finlay, D.K., Rosenzweig, E., Sinclair, L.V., Feijoo-Carnero, C., Hukelmann, J.L., Rolf, J., Panteleyev, A.A., Okkenhaug, K., and Cantrell, D.A. (2012). PDK1 regulation of mTOR and hypoxia-inducible factor 1 integrate metabolism and migration of CD8+ T cells. J. Exp. Med. *209*, 2441–2453. https://doi.org/10.1084/jem.20112607.

45. Wang, R., Dillon, C.P., Shi, L.Z., Milasta, S., Carter, R., Finkelstein, D., McCormick, L.L., Fitzgerald, P., Chi, H., Munger, J., and Green, D.R. (2011). The transcription factor Myc controls metabolic reprogramming upon T lymphocyte activation. Immunity *35*, 871–882. https://doi.org/10.1016/j.immuni.2011.09.021.

46. Pang, N., Duan, X., Jiang, M., Qu, J., Yuan, H., Xu, J., Cao, H., and Chen, G. (2015). Reconstitution and clinical significance of T cell subsets in the early stage after related HLA-mismatched peripheral blood hematopoietic SCT without T-cell depletion in vitro. Int. J. Clin. Exp. Pathol. *8*, 8892–8901.

47. Budde, H., Papert, S., Maas, J.H., Reichardt, H.M., Wulf, G., Hasenkamp, J., Riggert, J., and Legler, T.J. (2017). Prediction of graft-versus-host disease: a biomarker panel based on lymphocytes and cytokines. Ann. Hematol. *96*, 1127–1133. https://doi.org/10.1007/s00277-017-2999-5.

48. Martin, P.J. (1993). Donor CD8 cells prevent allogeneic marrow graft rejection in mice: potential implications for marrow transplantation in humans. J. Exp. Med. *178*, 703–712.

49. Graubert, T.A., DiPersio, J.F., Russell, J.H., and Ley, T.J. (1997). Perforin/granzyme-dependent and independent mechanisms are both important for the development of graft-versus-host disease after murine bone marrow transplantation. J. Clin. Invest. *100*, 904–911. https://doi.org/10.1172/JCI119606.

50. Sharpe, A.H., Wherry, E.J., Ahmed, R., and Freeman, G.J. (2007). The function of programmed cell death 1 and its ligands in regulating

autoimmunity and infection. Nat. Immunol. *8*, 239–245. https://doi.org/10.1038/ni1443.

51. Dong, H., Zhu, G., Tamada, K., and Chen, L. (1999). B7-H1, a third member of the B7 family, co-stimulates T-cell proliferation and interleukin-10 secretion. Nat. Med. *5*, 1365–1369. https://doi.org/10.1038/70932.

52. Saha, A., Aoyama, K., Taylor, P.A., Koehn, B.H., Veenstra, R.G., Panoskaltsis-Mortari, A., Munn, D.H., Murphy, W.J., Azuma, M., Yagita, H., et al. (2013). Host programmed death ligand 1 is dominant over programmed death ligand 2 expression in regulating graft-versus-host disease lethality. Blood *122*, 3062–3073. https://doi.org/10.1182/blood-2013-05-500801.

53. Wu, Y., Mealer, C., Schutt, S., Wilson, C.L., Bastian, D., Sofi, M.H., Zhang, M., Luo, Z., Choi, H.J., Yang, K., et al. (2022). MicroRNA-31 regulates T-cell metabolism via HIF1alpha and promotes chronic GVHD pathogenesis in mice. Blood Adv. *6*, 3036–3052. https://doi.org/10.1182/bloodadvances.2021005103.

54. Noman, M.Z., Desantis, G., Janji, B., Hasmim, M., Karray, S., Dessen, P., Bronte, V., and Chouaib, S. (2014). PD-L1 is a novel direct target of HIF-1alpha, and its blockade under hypoxia enhanced MDSC-mediated T cell activation. J. Exp. Med. *211*, 781–790. https://doi.org/10.1084/jem.20131916.

55. Zhao, D., Young, J.S., Chen, Y.H., Shen, E., Yi, T., Todorov, I., Chu, P.G., Forman, S.J., and Zeng, D. (2011). Alloimmune response results in expansion of autoreactive donor CD4+ T cells in transplants that can mediate chronic graft-versus-host disease. J. Immunol. *186*, 856–868. https://doi.org/10.4049/jimmunol.1002195.

56. Khuat, L.T., Le, C.T., Pai, C.C.S., Shields-Cutler, R.R., Holtan, S.G., Rashidi, A., Parker, S.L., Knights, D., Luna, J.I., Dunai, C., et al. (2020). Obesity induces gut microbiota alterations and augments acute graft-versus-host disease after allogeneic stem cell transplantation. Sci. Transl. Med. *12*, eaay7713. https://doi.org/10.1126/scitranslmed.aay7713.

57. Cetkovic-Cvrlje, M., Roers, B.A., Waurzyniak, B., Liu, X.P., and Uckun, F.M. (2001). Targeting Janus kinase 3 to attenuate the severity of acute graft-versus-host disease across the major histocompatibility barrier in mice. Blood *98*, 1607–1613. https://doi.org/10.1182/blood.v98.5.1607.

58. Cooke, K.R., Kobzik, L., Martin, T.R., Brewer, J., Delmonte, J., Jr., Crawford, J.M., and Ferrara, J.L. (1996). An experimental model of idiopathic pneumonia syndrome after bone marrow transplantation: I. The roles of minor H antigens and endotoxin. Blood *88*, 3230–3239.

STAR★METHODS

KEY RESOURCES TABLE

REAGENT or RESOURCE	SOURCE	IDENTIFIER
Antibodies		
Rat monoclonal anti-mouse PDL1	BioXCell	10F.9G2; RRID: AB_10949073
Rat monoclonal anti-mouse PD1	BioXCell	RMP1-14; RRID: AB_10949053
Rat monoclonal anti-mouse IFNγ	BioXCell	XMG1.2; RRID: AB_1107694
Mouse monoclonal anti-human PDL1	BioXCell	29E.2A3; RRID: AB_2687808
Rat monoclonal anti-keyhole limpet hemocyanin	BioXCell	LTF-2; RRID: AB_1107780
Ipilimumab	LakePharma	www.drugbank.ca/drugs/DB06186
fluoresceinisothiocyanate (FITC) conjugated anti-mouse CD45.1	eBioscience	11-0453-82; RRID: AB_465058
FITC conjugated anti-mouse CD45.2	eBioscience	11–0454-82; RRID: AB_465061
phycoerythrin (PE) conjugated anti–human CD45	eBioscience	12-0451-83; RRID: AB_465669
PE conjugated anti-mouse CD80	eBioscience	12-0801-82; RRID: AB_465752
PE conjugated anti-mouse CD8	eBioscience	12-0081-82; RRID: AB_465530
PE conjugated anti-mouse PDL1	eBioscience	12-5982-82; RRID: AB_466089
PE-Cy7 conjugated anti–human CD4	eBioscience	25-0047-42; 25-0047-42
PE-Cy7 conjugated anti-mouse CD4	eBioscience	25-0042-82; RRID: AB_469578
peridinin chlorophyll protein complex (PerCP) conjugated anti–mouse CD45.2	eBioscience	45-0454-82; RRID: AB_953590
PerCP conjugated anti-mouse Foxp3	eBioscience	45-5773-82; RRID: AB_914351
PerCP conjugated anti-mouse CD45.1	eBioscience	45-0453-82; RRID: AB_1107003
PerCP conjugated anti-mouse CD45	eBioscience	45-0451-82; RRID:AB_1107002
PerCP conjugated anti-mouse CD62L	eBioscience	45-0621-82; RRID: AB_996667
eFluor 450 conjugated anti-mouse CD3	eBioscience	48-0032-82; RRID: AB_1272193
APC-eFluor 780 conjugated anti-mouse CD44	eBioscience	47-0441-82; RRID: AB_1272244
PerCP conjugated anti-mouse CD8	BioLegend	100732; RRID: AB_893423
FITC conjugated anti-human CD8	BioLegend	344704; RRID: AB_1877178
FITC conjugated anti-mouse H-2D^{d}	BioLegend	110606; RRID: AB_10859623
PE-Cy 7 conjugated anti-human CD11b	BioLegend	393104; RRID: AB_2734451
APC conjugated anti-mouse IFNγ	BioLegend	505810; RRID: AB_315404
APC conjugated anti-mouse PD-L1	BioLegend	124312; RRID: AB_10612741
SparkBlue-550 anti-mouse CD3	BioLegend	100260; RRID: AB_2832258
BV510 conjugated anti-mouse CD45.2	BD Bioscience	740131; RRID: AB_2739888
BUV805 conjugated anti-mouse CD4	BD Bioscience	741913; RRID: AB_2871227
BUV563 conjugated anti-mouse CD8	BD Bioscience	752637; RRID: AB_2917622
PE conjugated anti-human HIF1α	RD Systems	IC1935P; RRID: AB_2232941
PerCP conjugated anti-human HIF1α	RD Systems	IC1935C
APC conjugated anti-human HIF1α	RD Systems	IC1935A; RRID: AB_1061580
Anti-human CD3	(NBP1, Novus)	NBP1-79054; RRID: AB_11015279
Anti-mouse CD3	(SP7, abcam)	Ab16669; RRID: AB_443425
Anti-cleaved caspase 3	(Asp175, 5A1E)	9664; RRID: AB_2070042

(*Continued on next page*)

Continued

REAGENT or RESOURCE	SOURCE	IDENTIFIER
Biological samples		
Human BM mononuclear cells	Stemcell Technologies	Catalog #: 70001.3
Human BM mononuclear cells	Lonza	Catalog #: 2M-125C
Chemicals, peptides, and recombinant proteins		
Echinomycin	Laboratory of Dr. Yin Wang	N/A
D-Luciferin potassium salt	GoldBio	LUCK-1G
Experimental models: Cell lines		
P815	ATCC	TIB-64; RRID: CVCL_2154
BLC1	ATCC	TIB-197; RRID: CVCL_4119
THP1	ATCC	TIB-202; RRID: CVCL_0006
K562	ATCC	CRL-3344; RRID: CVCL_UC14
KASUMI	ATCC	CRL-2724; RRID: CVCL_0589
Experimental models: Organisms/strains		
Mouse: *Nod.Scid.Il2rg*^{0} (NSG)	The Jackson Laboratory	Stock No. 005557; RRID: IMSR_JAX:005557
Mouse: *Hif1a*$^{flox/flox}$	The Jackson Laboratory	Stock No. 007561; RRID: IMSR_JAX:007561
Mouse: CD4^{Cre}	Charles River Laboratories	Stock No. 017336; RRID: IMSR_JAX:017336
Mouse: C57BL/6 (H-2^{b}, CD45.2^{+})	Charles River Laboratories	Strain Code: 027; RRID: IMSR_CRL:027
Mouse: B6-Ly5.2/Cr (H-2^{b}, CD45.1^{+})	Charles River Laboratories	Strain Code 494; RRID: IMSR_CRL:494
Mouse: BALB/c (H-2^{d})	Charles River Laboratories	Strain Code 028; RRID: IMSR_CRL:028
Mouse: CTLA4$^{h/h}$-KI	Laboratory of Dr. Yin Wang	N/A
Software and algorithms		
Living Image (Part Number 128110, IVIS Lumina Series)	Perkin Elmer	https://www.perkinelmer.com/product/li-software-for-lumina-1-seat-add-on-128110
Prism 8	GraphPad	https://www.graphpad.com/
Other		
Prolong Antifade mounting buffer	Invitrogen	P36980

RESOURCE AVAILABILITY

Lead contact

Further information and requests for resources and reagents should be directed to and will be fulfilled by the lead contact, Yin Wang (yin.wang@ihv.umaryland.com).

Materials availability

This study did not generate new unique reagents.

Data and code availability

- Data generated and/or analyzed in this study, excluding identifying personal information, are available from the lead contact, Yin Wang (yin.wang@ihv.umaryland.edu) with reasonable request to protect research participant privacy.
- This paper does not report original code.
- Any additional information required to reanalyze the data reported in this paper is available from the lead contact upon request.

EXPERIMENTAL MODEL AND STUDY PARTICIPANT DETAILS

Mice

All procedures involving experimental animals were approved by Institutional Animal Care and Use Committees (IACUC) of the Children's Research Institute and the University of Maryland School of Medicine where this work was performed. *Nod.Scid.Il2rg*^{0} (NSG), *Hif1a*$^{flox/flox}$ and CD4^{Cre} mice were purchased from the Jackson Laboratory. C57BL/6 (H-2^{d}, CD45.2^{+}), B6-Ly5.2/Cr (H-2^{b}, CD45.1^{+}) and BALB/c (H-2^{d}) mice were purchased from Charles River Laboratories. CTLA4$^{h/h}$-KI mice were generated and bred in-house and

have been previously described.[41] Male and female mice were used for all studies. For allogeneic models, 8–10 weeks old donor and recipient mice were used and animals of the same sex were randomly assigned to treatment groups within a single experiment. For the xenogeneic model, newborn pups (3–5 days old) were used and animals were assigned to treatment groups by selecting roughly equal number of male and female littermates and, in the case of multiple litters, a roughly equal distribution of animals from each litter. Animals were group housed and maintained under standard conditions (temperature, humidity, and light controlled, and standard diet) for mouse research at the Research Animal Facilities at Children's Research Institute or University of Maryland School of Medicine. None of the animals selected for experiments had received prior treatment or were involved in any previous procedures.

METHOD DETAILS

Allogeneic mouse model of GVHD and GVL

Lethally irradiated (8.50-Gy split-dosed) BALB/c mice were reconstituted with 3–5 X10^5 of either WT or *Hif1a*$^{-/-}$ T cells, mixed with 5X10^6 TCD BM from B6-Ly5.2/Cr mice. For experiments using *CTLA4*$^{h/h}$ T cells, the same parameters were used except for the T cells were isolated from the WT or *Hif1a*$^{-/-}$ *CTLA4*$^{h/h}$ donors. For the GVL models, 1X10^3 P815 cells were intravenously injected into BALB/c mice 12 h after lethal irradiation. For BCL1, the same procedure was used except that the mice received 5X10^6 BCL1 cells per mouse, injected intraperitoneally. For both models, bioluminescence imaging was used to confirm and monitor leukemia growth. Recipients were also monitored daily for clinical signs of GVHD by body weight and visible skin pathology. For experiments involving drug treatment, the mice received antibodies at 0.2 mg/mouse (anti-mouse PDL1, 10F.9G2; anti-mouse PD1, RMP1-14; anti-IFNγ, XMG1.2; anti-human CTLA-4, Ipilimumab), and Echinomycin (EM) at 0.01 mg/kg, by intraperitoneal injection. In some experiments, the animals received echinomycin in liposomal form (abbreviated LEM), the dose is the same.

Xenogeneic GVHD and GVL model

Human BM mononuclear cells isolated from healthy adult human BM using density gradient separation were purchased from Stemcell Technologies (Vancouver, Canada) and Lonza (Walkersville, MD, USA). 0.1–0.5X10^6 cells were transplanted via intrahepatic injection into irradiated (1.30 Gy) newborn NSG pups. Human CD45$^+$CD3$^+$ cells in PBL of recipients were detected by FACS analysis. For the GVL model, NSG pups received 1X10^6 of luciferase transduced human THP1 intrahepatically at day 2 postnatal and then received 0.35X10^6 human BM cells intrahepatically. For *in vivo* PDL1 antibody treatment, the recipients received 3 intraperitoneal injections of anti-mouse PDL1 (10F.9G2), anti-human PDL1 (29E.2A3), or isotype control IgG (LTF-2) (BioxCell, West Lebanon, NH) starting on day 7 after BMT at a dose of 50 μg/mouse.

Gene set enrichment analysis (GSEA)

GSEA calculations were performed with the GSEA program (v. 3.0). The Broad Molecular Signatures Database (MSigDB v6.0) set H (hallmark gene sets) was used. Hallmark gene sets summarize and represent specific well-defined biological states or processes and display coherent expression. For GVHD patients (11 cases) compared with Non-GVHD patients (13 cases), the GSEA involved HIF1α target genes and 50 hallmark gene sets. The GSEA program was run with 1,000 permutations for statistical significance estimation, and the default signal-to-noise metric between the two phenotypes was used to rank all genes. In the heatmap generated by GSEA, expression values are represented as colors, where the range of colors (red, pink, light blue, dark blue) shows the range of expression values (high, moderate, low, lowest).

Gene transcript analysis of patient samples

The mononuclear cells from peripheral blood or BM from GVHD and Non-GVHD HSCT patients were obtained from the Second Hospital of Dalian Medical University at Dalian in China. The collection of patient samples was approved by the Second Hospital of Dalian Medical University Institutional Review Board. mRNA was isolated from PBMC or BM, and reverse transcription and real-time PCR was performed per manufacturer's recommendations (Applied biosystems, Foster City, CA, USA). The clinical characteristics of GVHD and Non-GVHD patients and the primer sequences are listed in Tables S1 and S3.

Flow cytometry

Peripheral blood was collected by sub-mandibular bleeding at different times after BMT. Fluorochrome-labeled antibodies were directly added into whole blood. After 30 min of staining, the samples were treated with BD FACS Lysing Solution to lyse the red blood cells and washed twice with DPBS (1X) before analysis. Spleens and BM were dissociated using frosted microscope slides and syringes, respectively, to obtain single-cell suspensions. The samples were passed through a nylon cell strainer, washed three times with RPMI-1640, stained with antibodies, and then analyzed on flow cytometry for different human cell populations. Antibodies used were fluoresceinisothiocyanate (FITC) conjugated anti-mouse CD45.1, and CD45.2; phycoerythrin (PE) conjugated anti–human CD45, anti-mouse CD80, anti-mouse CD8, and anti-mouse PD-L1; PE-Cy7 conjugated anti–human CD4, anti-mouse CD4; peridinin chlorophyll protein complex (PerCP) conjugated anti–mouse CD45.2, anti-mouse Foxp3, anti-mouse CD45.1, anti-mouse CD45, and anti-mouse CD62L; eFluor 450 conjugated anti-mouse CD3; APC-eFluor 780 conjugated anti-mouse CD44, (eBioscience, San Diego, CA), PerCP conjugated anti-mouse CD8, FITC conjugated anti-human CD8, anti-mouse H-2D^d, PE-Cy 7 conjugated anti-human CD11b, APC conjugated anti-mouse IFNγ and anti-mouse PD-L1 (BioLegend). BUV and BV series antibodies used for Cytek

Aurora included the following (all from BD Bioscience, San Jose, CA): BV510 anti-mouse CD45.2, BUV805 anti-mouse CD4, BUV563 anti-mouse CD8. We also used SparkBlue-550 anti-mouse CD3 (BioLegend), and PE, PerCP and APC conjugated anti-human HIF1α from RD Systems (Minneapolis, NM). The stained cells were analyzed using the BD FACS Canto II or Cytek Aurora flow cytometers.

Immunofluorescence staining

Tissues harvested from the mice were fixed in 10% neutral-buffered formalin before embedding in paraffin blocks and cutting into 4-μm sections. After deparaffinization and rehydration with xylene and ethanol, tissue sections were treated with 10 mM sodium citrate buffer, pH 6.0. The sections were permeabilized with 0.3% Triton X-100 in 10 mM Tris-HCl buffer for 30 min. After blocking with 2% bovine serum albumin (BSA) for 60 min, sections were incubated with primary antibody diluted in 10 mM Tris-HCl buffer containing 2% BSA at 4°C, overnight, with subsequent staining with secondary antibody in BSA-Tris-HCl buffer at room temperature for 2–4 h. The nuclei were stained with DAPI. Slides were mounted with Prolong Antifade mounting buffer (Invitrogen, Carlsbad, CA 92008). Antibodies for hCD3 (NBP1, Novus), mCD3 (SP7, abcam), cleaved caspase-3 (Asp175, 5A1E), and mPD-L1 (10F.9G2, BioxCell, West Lebanon, NH) were used for immunofluorescence.

Pathology scores

Slides were stained with hematoxylin and eosin (H&E) and examined in double-blinded fashion. Histopathological scores were evaluated according to the publications.[55–57] GVHD scores were assigned to the tissues according to the following criteria. Liver GVHD was scored on a scale of 0–16, based on infiltration (0–4), portal fibrosis (0–4), damage of epithelium of bile duct (0–4) and cytoplasmic vacuolation (0–4). Kidney GVHD was scored on a scale of 0–8, based on infiltration (0–4) and swelling and necrosis of tubules (0–4). Intestine GVHD was scored on a scale of 0–12, based on infiltration (0–4), depth of damage (0–4) and absence of intestinal villus (0–4). Lung GVHD was scored on a scale of 0–12, based on infiltration (0–4), alveolar damage (0–4) and bronchiolar epithelial hyperplasia and detachment (0–4). Salivary gland GVHD was scored on a scale of 0–8, based on infiltration (0–4) and granular atrophy and tissue destruction (0–4). Infiltration was graded on the number of foci: 1 stands for 1–3 small foci composed of mononuclear cells per section. 2 stands for 4–10 small foci. 3 stands for 10–20 small foci. 4 stands for more than 20 small foci. Tissue damage was graded on the ratio of damaged part to normal part: 1 stands for less than 10% per section. 2 stands for 10%–25%. 3 stands for 25%–50%. 4 stands for more than 50%.

Clinical GVHD assessment

The severity of systemic GVHD developed in the mice was assessed according to a mouse clinical GVHD scoring system, which was first described by Cooke et al.[58] Briefly, GVHD was assessed based on five clinical parameters on a scale from 0 to 2 according to severity: weight loss (grade 1, 10–25%; grade 2, >25%), posture (1, hunching noted only at rest; 2, stationary unless stimulated), activity (1, stationary >50% of the time; 2, stationary unless stimulated), fur texture (1, mild to moderate fur ruffling; 2, ruffling entire body), and skin integrity (1, scaling paws/tail/anus; 2, multiple open lesions). Each mouse's total clinical GVHD score was generated by summation of the five criteria scores (0–10) at different timepoints after BMT.

Bioluminescence imaging

Luciferase activity was analyzed in mice anesthetized with isoflurane 10 min after intraperitoneal injection 150 mg/kg of D-luciferin potassium salt (GoldBio). Mice were imaged in a Xenogen IVIS Spectrum Imaging System (Caliper Life Sciences). Living Image software was used to analyze the bioluminescent image data. Total bioluminescent signal was obtained as photons/second and regions of interest were used to calculate regional signals.

QUANTIFICATION AND STATISTICAL ANALYSIS

All experiments were performed at least twice with similar results. Appropriate statistical tests were selected on the basis of whether the data with outlier deletion was normally distributed by using the D'Agostino & Pearson normality test. Data comparing 2 groups were analyzed by unpaired, 2-tailed Student's *t* test. 1-way analysis of variance (ANOVA) with Sidak's post hoc test was used for data comparing multiple groups, and two-way ANOVA for data time-course studies. The correlation coefficient and p value for linear regression were calculated by Pearson's method. Sample sizes were chosen with adequate statistical power on the basis of the literature and past experience. In the graphs, data are shown as mean ± SEM, indicated by horizontal line and y axis error bars, respectively. Statistical calculations were performed using Prism 8 software (GraphPad Software). NS in the figures indicates no significant difference. A p value of less than 0.05 was considered significant: *$p < 0.05$, **$p < 0.01$, ***$p < 0.001$, ****$p < 0.0001$.